SEMESTER THESIS

Linearized Reactive Flow with Equivalence Ratio Perturbations

Autor:
Maximilian Kühn

Matrikel-No:
3624202

Betreuer:
Alexander Avdonin, M. Sc.
Prof. Wolfgang Polifke, Ph. D.

January 15, 2018

Technische Universität München
Fakultät für Maschinenwesen
Professur für Thermofluiddynamik
Prof. Wolfgang Polifke, Ph. D.

Erklärung

Hiermit versichere ich, die vorliegende Arbeit selbstständig verfasst zu haben. Ich habe keine anderen Quellen und Hilfsmittel als die angegebenen verwendet.

Ort, Datum	Maximilian Kühn

Abstract

This thesis investigates a numerical method to quickly assess the response of a laminar, premixed flame to equivalence ratio perturbations. This linearized reacting flow (LRF) solver relies on linearizing Navier-Stokes equations with reacting species equations. The governing equations are linearized around a steady operation point, while reaction and heat release terms are expressed with a linearized Arrhenius equation. The number of independent variables is kept low by exploiting analytic correlations from the reaction equation. Discretization is done by the discontinuous Galerkin finite element method. The linear system of equations is solved in frequency domain with the simulation software COMSOL 4.4 to compute the flame response functions (FRF).

The LRF solver is applied to investigate attached and lifted laminar premixed flames in 2D for equivalence ratio perturbations. Results are compared to FRF identified from a CFD simulation. The phase of simulated FRFs is in excellent agreement with the reference data from CFD. Gain, however, is underestimated by the LRF solver for the attached flame and falsely predicts the excessive gain peak frequency for the lifted flame. Secondly, the LRF solver's solution is examined towards the influence of mass fraction perturbations on enthalpy and temperature perturbations. Results show, that temperature is not influenced by mass fraction perturbations, while mass fraction perturbations have to be modelled for enthalpy perturbations.

Contents

List of Figures

List of Tables

Nomenclature

Roman Symbols

$[X_k]$	Molecular concentration of species k	[mol m^{-3}]
Le	Lewis number	[-]
Pr	Prandtl number	[-]
Sc	Schmidt number	[-]
$\Delta h^0_{f,k}$	Standard enthalpy of formation	[J kg^{-1}]
$\mathscr{M}_k$	Chemical symbol of species k	[-]
$\mathscr{Q}_n$	Rate of progress for reaction n	[mol m$^{-3}s^{-1}$]
$\mathscr{R}$	Universal gas constant	[J mol$^{-1}K^{-1}$]
A_S	Sutherland constant	[kg m$^{-1}s^{-1}K^{-\frac{1}{2}}$]
A_n	Arrhenius constant of reaction n	[cgs units]
c	Speed of sound	[m s^{-1}]
D_k	Diffusion coefficient of species k	[kg m$^{-1}s^{-1}$]
E_a	Activation energy	[J mol^{-1}]
F_u	FRF for velocity perturbations	[-]
F_ϕ	FRF for equivalence ratio perturbations	[-]
h	Sensible enthalpy	[J kg^{-1}]
$k_{\sum Y'}$	Coeffient in sum of mass fractions	[-]
$K_{f/r,n}$	Forward/reverse rate of reaction n	[s^{-1}]
l_{φ_i}	FEM ansatz function for variable φ_i	[-]

n_i	Element boundary vector normal component in i-direction	[-]
p	Pressure	[Pa]
R_k	Specific gas constant of species k	[J kg$^{-1}K^{-1}$]
s	Stoichiometric mass ratio	[-]
S_{φ_i}	Source term in conservation equation for φ_i	[-]
T	Temperature	[K]
t	Time	[s]
T_a	Activation temperature	[K]
T_S	Sutherland temperature	[K]
T_{ref}	Reference temperature	[K]
u	Velocity in x-direction	[m s^{-1}]
v	Velocity in y-direction	[m s^{-1}]
W	Mean molecular weight	[kg mol^{-1}]
W_k	Molecular weight of species k	[kg mol^{-1}]
Y	Mass fraction of methane CH_4	[-]
Y_k	Mass fraction of species k	[-]
Z	Mass fraction of nitrogen N_2	[-]

Greek Symbols

$\dot{\omega}_k$	Reaction rate of species k	[kg m$^{-3}s^{-1}$]
$\dot{\omega}_T$	Heat release rate	[W m^{-3}]
α	Thermal diffusivity	[kg m$^{-1}s^{-1}$]
β	Temperature exponent	[-]
δ_{ij}	Kronecker delta	[-]
Γ_e	Element boundary (line in 2D)	[m]
κ	Ratio of specific heats	[-]
μ	Dynamic viscosity	[kg m$^{-1}s^{-1}$]

ν_{kn}	Stoichiometric coefficient of species k in reaction n	[-]
Ω	Computational domain volume (area in 2D)	[m^2]
Ω_e	Element volume (area in 2D)	[m^2]
ϕ	Equivalence ratio	[-]
$\boldsymbol{\varphi}$	Field variable vector	[-]
Ψ_j	Flux in j-direction	[-]
ρ	Density	[kg m^{-3}]
τ_{ij}	Viscous stress tensor	[kg $m^{-1} s^{-2}$]
φ_i	Transport variable	[-]
ξ	Progress variable	[-]

Miscellaneous

$\frac{\partial}{\partial x_i / t}$	Partial differential in space/time	[-]
∇	Nabla operator	[-]
$\overline{()}$	Mean flow value	[-]
$()'$	Perturbation value	[-]
$()_0$	Inlet condition	[-]

Acronyms

BC	Boundary condition
DG	Discontinunous Galerkin
DOF	Degree of freedom
FEM	Finite element method
FIR	Finite impulse response
FRF	Flame response function
FTF	Flame transfer function
FVM	Finite volume method
HO	Higher order

JANAF	Joint Army Navy NASA Air Force (Interagency Propulsion Committee)
LIGL	Linearized ideal gas law
LNSE	Linearized Navier-Stokes equations
LRF	Linearized reacting flow
MVP	Mean value property
NSE	Navier-Stokes equations
PDE	Partial differential equation

1 Introduction

The first chapter will explain: Why is this topic interesting? How are similar problems investigated and what improvements are possible? At the end of the chapter, the thesis structure is outlined for the reader's overview.

For the steady supply of power in electricity generation or propulsion, gas turbines are a widely spread technology. Their design and optimization commands a high attention from both academic and industry researchers. Within this research, the study of the thermoacoustic properties of combustion chambers is a field of particular interest, as emission specifications are becoming increasingly strict. This requires operation at lean conditions, where gas turbines tend to instabilities. These arise from feedback interaction of hear release rate, flow and acoustics. The coupling effects of burner flames and acoustic waves are therefore to be carefully considered in the design of modern combustion systems, such as aircraft and rocket engines or stationary power and heat supply.

Instabilities can cause a number of effects, that can be harmful: oscillations in flow parameters (velocities, pressure, temperature, etc.), increasing amplitudes of flame movement and heat transfer to walls, destruction of combustion chamber parts, or loss of system control. In general, development aims at avoiding and controlling unstable flame regimes. (cf. [3])

Premixed flame combustors are usually designed to operate at a stable design point with a premixed flame whose flow may be laminar or stabilized by turbulence (swirl-stabilization).

1.1 Flame Transfer Functions in Stability Analysis

The flow-flame interaction often represented by a flame response function (FRF) which relate a flame's heat release fluctuations $\dot{Q}'$ to perturbations of velocity or to equivalence ratio perturbations upstream of the flame. For the case of velocity perturbations, the flame response function is also referred to as flame transfer function (FTF). This definition reads:

$$\text{Velocity perturbations:} \qquad \frac{\dot{Q}'}{\overline{\dot{Q}}} = F_u \frac{u'_{\text{ref}}}{\overline{u}_{\text{ref}}} \tag{1.1}$$

$$\text{Equivalence ratio perturbations:} \qquad \frac{\dot{Q}'}{\overline{\dot{Q}}} = F_\phi \frac{\phi'_{\text{ref}}}{\overline{\phi}_{\text{ref}}} \tag{1.2}$$

Note, that this formulation omits that heat release rate terms are taken as intergrals over the entire domain, while the flow variables are point values at a fixed reference point.

On equivalence ratio perturbations, Albayrak et al. [4] repeat the danger of uncontrolled, large amplitude oscillations in combustion chambers. The authors also state that 'perturba-

tions in equivalence ratio modulate the heat of reaction and the laminar flame speed, which affect the heat release rate of the flame in a direct manner' [4, p. 3726]. This correlation was discovered by Dowling and Hubbard [5] in 2000. Further research on the topic of fuel-air ratio oscillations was carried out by Cho and Lieuwen [6], Shreekrishna et al. [7] and Hemchandra [8].

Even though computational resources are constantly increasing, highly resolved LES of e.g. a turbine combustor is still too expensive for industrial development. In order to downsize the problem, hybrid approaches are taken, that couple acoustic models with a FRF. (cf. for instance [9, 10, 11]). Then the identification of the flame response to perturbations is typically done from time series data, that is computed with rather costly CFD methods [12, 13].

In the popular thermoacoustic network models the combustion chamber is modelled as a series of ducts or area jumps, through which acoustic waves travel. Owing to better algorithms and computing power, the resolution of the acoustic field in a combustor is now possible with two- or three-dimensional simulation of the Helmholtz, linearized Euler or the linearized Navier-Stokes equations. The flame dynamics is in all models introduced by a FRF, that has to be previously identified.

Recent work by Avdonin et al. [14] introduces a method, that is not relying on externally provided FTFs. Here, the Navier-Stokes and reacting species equations are analytically linearized to obtain linearized reacting flow (LRF). The LRF solver uses the discontinuous Galerkin finite element discretization and operates in the frequency domain. Besides CFD simulation to generate the mean fields, no further input is needed.

Earlier works by van Kampen et al. [15] on flame response to equivalence ratio perturbations and by Blanchard et al. [16] on the effects of flow fluctuations on the flame also operate with linearization techniques. Their approach is, however, to numerically linearize the governing equations and compute FRFs as step response in the time domain.

This thesis aims to show that LRF could be used for equivalence ratio perturbations in laminar, premixed flames.

1.2 Motivation and Outline

The main goal of the presented work is to investigate LRF as a method for computing FRFs, that is computationally less expensive than LES and still displays flame-acoustics interaction accurately. Even though computing power has been permanently increasing over the last decades and simulation of complete combustion chambers in three dimensions is now possible, CFD simulation of reactive flow fields in high resolution (LES or DNS) is still available for only few reference cases and at high costs. With the demand for new, less emissive turbines, a feasible alternative for daily application in R&D departments is sought after.

The simulation model based on linearization of the governing equations could show to be a candidate for fast identification of FTFs. Deduction and application of the LRF approach to equivalence ratio perturbations is presented in this thesis.

The next chapter will explain, how the Navier-Stokes equations (NSE) are linearized with first order Taylor expansion and acting forces terms like diffusion or sources are modelled. At

the end we obtain so called linearized reacting flow (LRF) equations.

Chapter 3 will describe, how the number of independent variables is reduced by utilizing the chemical reaction of the combustion. Thus, the number of degrees of freedom and thereby computational effort is reduced.

The linearized governing equations for methane combustion are then discretized by the discontinuous Galerkin finite element method. The discontinuous Galerkin form of the LRF is described in chapter 4.

Thereafter, in chapter 5, the numerical setup with the software COMSOL Multiphysics 4.4 is introduced. Geometry, meshing, and boundary conditions are shown and the simulation procedure described. Afterwards, the numerical model is applied to study attached and lifted laminar premixed flames. The main part will focus on the model's performance in computing the FRF for equivalence ratio perturbations. The results are discussed in terms of accuracy in gain and phase of frequency responses. Secondly, influence of mass fraction perturbations in linearized terms for temperature and enthalpy are examined.

Finally the thesis is concluded with a review the work done and ideas for future work.

Appendixes give detailed formula and explanations, where needed, and are referenced in the text.

2 Linearization of the 2D compressible Navier-Stokes equations

At the base of our approach is the linearization of the Navier-Stokes equations (NSE), the ideal gas law, and the included material properties. This procedure is explained in detail in the following chapter.

2.1 The non-linear Navier-Stokes equations

The full compressible NSE describe the behaviour of a fluid as a continuum. These are linearized to obtain the LRF equations. The non-linear conservation laws are solved in the OpenFOAM solver in this form:

$$\begin{aligned}
\text{Mass:} \quad & \frac{\partial \rho}{\partial t} + \frac{\partial \rho u_i}{\partial x_i} = 0 \\
\text{Momentum:} \quad & \frac{\partial \rho u_i}{\partial t} + \frac{\partial \rho u_i u_j}{\partial x_j} = -\frac{\partial p}{\partial x_i} + \frac{\partial \tau_{ij}}{\partial x_j} \\
\text{Species:} \quad & \frac{\partial \rho Y_k}{\partial t} + \frac{\partial \rho u_j Y_k}{\partial x_j} = \frac{\partial}{\partial x_j}\left(D_k \frac{\partial Y_k}{\partial x_j}\right) + \dot{\omega}_k \\
\text{Sensible enthalpy:} \quad & \frac{\partial}{\partial t}\left(\rho h - p\right) + \frac{\partial \rho u_i h}{\partial x_i} = \dot{\omega}_T + \frac{\partial}{\partial x_i}\left(\alpha \frac{\partial h}{\partial x_i}\right).
\end{aligned} \tag{2.1}$$

Here, $\frac{\partial}{\partial t}$ denotes the time derivative and $\frac{\partial}{\partial x_i}$ the space derivative in Cartesian coordinate direction i. The conservation of sensible enthalpy is taken from [17] (`eq. 13`), but kinetic energy and viscous terms are omitted. This thesis follows the OpenFOAM definitions of mass and thermal diffusivities, D_k and α, with SI-units kg/(ms).

Modelling Assumptions

The following assumptions are made in order to simplify the real physics, while keeping enough accuracy.

All fluids are treated as Newtonian fluids, i.e. the viscosity tensor entries are taken from Newton's law as

$$\tau_{ij} = \mu\left(\frac{\partial u_i}{\partial x_j} + \frac{\partial u_j}{\partial x_i} - \frac{2}{3}\delta_{ij}\frac{\partial u_k}{\partial x_k}\right)$$

with the Kronecker-Delta

$$\delta_{ij} = \begin{cases} 1, & \text{if } i = j, \\ 0, & \text{if } i \neq j. \end{cases}$$

Molecular diffusion in the species conservation equations is modelled by Fick's Law.

For modelling the temperature dependence of viscosity, Sutherland's law is applied. By assumption of a constant Prandtl number Pr:

$$\mathrm{Pr} = \frac{\mu}{\alpha} = 0.71$$

the thermal diffusion coefficient α is dependent on the modeling for μ. This assumption was earlier made even for turbulent premixed flames by Haworth and Poinsot [18, p. 411]. We also assume a unity Lewis number for all species and thereby get a constant Schmidt number Sc and expression for mass diffusivity D_k:

$$\mathrm{Sc} = \frac{\mu}{D_k} = 0.71$$

As OpenFOAM equations are solved, $-\alpha \frac{\partial h}{\partial x_i}$ is replacing $-\lambda \frac{\partial T}{\partial x_i}$, the common expression for heat flux in Fourier's law.

The ideal gas law for mixtures

$$p = \rho \, \mathscr{R} \, T \sum_k \frac{Y_k}{W_k}$$

is applied as a closure equation in linearized form to express temperature T by field variables $\boldsymbol{\varphi}$.

For the reaction rate $\dot{\omega}_k$ and heat release $\dot{\omega}_T$, a one-step chemical mechanism is assumed, as proposed by Westbrook and Dryer [19], and the rate of progress is described by a linearized Arrhenius formulation.

The sensible enthalpy h is defined from the integral formulation

$$h = \int_{T_{ref}}^{T} c_p(T, Y_k) \, dT$$

and the heat capacity $c_p(T, Y_k)$ is taken from the Joint Army-Navy-NASA-Air Force (JANAF) Interagency Propulsion Committee as a polynomial of 4th degree

$$c_p = \sum_k R_k \Big(\sum_{n=0}^{4} a_{n,k} T^n \Big) Y_k$$

Lastly, occurring species i are methane, oxygen, nitrogen, carbon dioxide, and water.

$$i \in \{CH_4, O_2, N_2, CO_2, H_2O\}$$

and air is - at the inflow - modelled a constant mixture of 78.8 $\%_{Vol}$ N_2 and 21.2 $\%_{Vol}$ O_2, while all other possible components (Ar, CO_2, etc.) are neglected.

Any further assumptions not given here, are explained en route as the model is derived. Also, more detailed mathematical expressions and further information are given, when the described simplifications are applied in the next section.

2.2 Linearization

The linearization approach assumes, that a steady-state mean flow is superimposed by time-variant perturbations. The mean flow is in our case generated by CFD simulation with OpenFOAM and taken as an input of constant fields.

Thus, equations (2.1) are linearized by the assumption that the field variables can be written as a sum of time-independent mean flow and time-dependent perturbations:

$$\begin{aligned} \rho(x,t) &= \overline{\rho}(x) + \rho'(x,t) \\ u(x,t) &= \overline{u}(x) + u'(x,t) \\ v(x,t) &= \overline{v}(x) + v'(x,t) \\ p(x,t) &= \overline{p}(x) + p'(x,t) \\ Y_k(x,t) &= \overline{Y}_k(x) + Y'_k(x,t) \end{aligned} \tag{2.2}$$

As a steady state with perturbations excited by fluctuations at the inlet is examined, the governing equations formulated in mean flow field variables ($\overline{\boldsymbol{\varphi}}$ only) remain valid. This characteristic is called mean value property (MVP) and allows us to disregard the terms with only $\overline{\boldsymbol{\varphi}}$ in the LNSE. As linearization is done with Taylor expansion to the first derivative, quadratic or higher order (HO) terms of perturbation are assumed small $\boldsymbol{\varphi'}^2 << \boldsymbol{\varphi'}$ and are therefore neglected.

These are combined in the field variable vector $\boldsymbol{\varphi}$ and perturbations are considered small in comparison to mean flow:

$$\boldsymbol{\varphi} = \begin{pmatrix} \rho \\ u \\ v \\ p \\ Y_{CH_4} \\ \vdots \end{pmatrix} = \underbrace{\begin{pmatrix} \overline{\rho} \\ \overline{u} \\ \overline{v} \\ \overline{p} \\ \overline{Y}_{CH_4} \\ \vdots \end{pmatrix}}_{\overline{\boldsymbol{\varphi}}} + \underbrace{\begin{pmatrix} \rho' \\ u' \\ v' \\ p' \\ Y'_{CH_4} \\ \vdots \end{pmatrix}}_{\boldsymbol{\varphi'}}$$

$$\overline{\boldsymbol{\varphi}} \;>>\; \boldsymbol{\varphi'}$$

Since material properties are highly temperature dependent, viscosity μ, diffusion coefficients D_k and thermal diffusivity α are linearized as well as sensible enthalpy h.

2.2.1 Continuity equation

The linearized continuity equation is obtained by inserting the terms for density and velocities from eq. (2.2) into the mass conservation from eq. (2.1):

$$\frac{\partial(\overline{\rho}+\rho')}{\partial t}+\frac{\partial(\overline{\rho}+\rho')(\overline{u}+u')}{\partial x}+\frac{\partial(\overline{\rho}+\rho')(\overline{v}+v')}{\partial y}=0 \tag{2.3}$$

$$\frac{\partial\overline{\rho}}{\partial t}+\frac{\partial\rho'}{\partial t}+\frac{\partial\overline{\rho u}}{\partial x}+\frac{\partial\rho'\overline{u}}{\partial x}+\frac{\partial\overline{\rho}u'}{\partial x}+\frac{\partial\rho'u'}{\partial x}+\frac{\partial\overline{\rho v}}{\partial y}+\frac{\partial\rho'\overline{v}}{\partial y}+\frac{\partial\overline{\rho}v'}{\partial y}+\frac{\partial\rho'v'}{\partial y}=0$$

$$\underbrace{\frac{\partial\overline{\rho}}{\partial t}+\frac{\partial\overline{\rho u}}{\partial x}+\frac{\partial\overline{\rho v}}{\partial y}}_{=0\text{ cf. MVP}}+\frac{\partial\rho'}{\partial t}+\frac{\partial\rho'\overline{u}}{\partial x}+\frac{\partial\overline{\rho}u'}{\partial x}+\frac{\partial\rho'\overline{v}}{\partial y}+\frac{\partial\overline{\rho}v'}{\partial y}+\underbrace{\cancel{\frac{\partial\rho'u'}{\partial x}}+\cancel{\frac{\partial\rho'v'}{\partial y}}}_{\text{HO terms}}=0$$

As described earlier, the conservation of mass for the mean values is unchanged allowing us to apply the MVP. The higher order terms containing non-linear combinations of perturbations are left out in order to obtain linearized conservation laws.

Finally, the linearized continuity equation reads:

$$\frac{\partial\rho'}{\partial t}+\frac{\partial\rho'\overline{u}}{\partial x}+\frac{\partial\overline{\rho}u'}{\partial x}+\frac{\partial\rho'\overline{v}}{\partial y}+\frac{\partial\overline{\rho}v'}{\partial y}=0 \tag{2.4}$$

2.2.2 Momentum equations

Similar to the previous section, the terms from eq. (2.2) are substituted into the momentum conservation equation in eq. (2.1).

The linearization technique is the same for conservation equations. The total flow variables from $\boldsymbol{\varphi}$ are replaced by the sum $\overline{\boldsymbol{\varphi}}+\boldsymbol{\varphi'}$ and all multiplications are fully expanded. Subsequently, the MVP is applied and HO terms cancelled out.

Detailed deductions of the linearized conservation laws can be found in Appendix A.

x-Momentum equation

$$\begin{aligned}&\frac{\partial\rho'\overline{u}}{\partial t}+\frac{\partial\overline{\rho}u'}{\partial t}+\frac{\partial\overline{\rho u}u'}{\partial x}+\frac{\partial\overline{\rho}u'\overline{u}}{\partial x}+\frac{\partial\rho'\overline{uu}}{\partial x}+\frac{\partial\overline{\rho u}v'}{\partial y}+\frac{\partial\overline{\rho}u'\overline{v}}{\partial y}+\frac{\partial\rho'\overline{uv}}{\partial y}=\\&-\frac{\partial p'}{\partial x}+\frac{\partial}{\partial x}\mu'\left(\frac{4}{3}\frac{\partial\overline{u}}{\partial x}-\frac{2}{3}\frac{\partial\overline{v}}{\partial y}\right)+\frac{\partial}{\partial x}\overline{\mu}\left(\frac{4}{3}\frac{\partial u'}{\partial x}-\frac{2}{3}\frac{\partial v'}{\partial y}\right)+\frac{\partial}{\partial y}\mu'\left(\frac{\partial\overline{u}}{\partial y}+\frac{\partial\overline{v}}{\partial x}\right)+\frac{\partial}{\partial y}\overline{\mu}\left(\frac{\partial u'}{\partial y}+\frac{\partial v'}{\partial x}\right)\end{aligned} \tag{2.5}$$

y-Momentum equation

$$\begin{aligned}&\frac{\partial\rho'\overline{v}}{\partial t}+\frac{\partial\overline{\rho}v'}{\partial t}+\frac{\partial\overline{\rho u}v'}{\partial x}+\frac{\partial\overline{\rho}u'\overline{v}}{\partial x}+\frac{\partial\rho'\overline{uv}}{\partial x}+\frac{\partial\overline{\rho v}v'}{\partial y}+\frac{\partial\overline{\rho}v'\overline{v}}{\partial y}+\frac{\partial\rho'\overline{vv}}{\partial y}=\\&-\frac{\partial p'}{\partial y}+\frac{\partial}{\partial y}\mu'\left(\frac{4}{3}\frac{\partial\overline{v}}{\partial y}-\frac{2}{3}\frac{\partial\overline{u}}{\partial x}\right)+\frac{\partial}{\partial y}\overline{\mu}\left(\frac{4}{3}\frac{\partial v'}{\partial y}-\frac{2}{3}\frac{\partial u'}{\partial x}\right)+\frac{\partial}{\partial x}\mu'\left(\frac{\partial\overline{u}}{\partial y}+\frac{\partial\overline{v}}{\partial x}\right)+\frac{\partial}{\partial x}\overline{\mu}\left(\frac{\partial u'}{\partial y}+\frac{\partial v'}{\partial x}\right)\end{aligned} \tag{2.6}$$

Linearization of dynamic viscosity μ and the ideal gas law

As mentioned in section 2.1, the dynamic viscosity μ is expressed by the formula introduced by Sutherland [20] in 1893:

$$\mu = \frac{A_S\sqrt{T}}{1+\frac{T_S}{T}} \tag{2.7}$$

with $A_S = 1.67212{\cdot}10^{-6}$ kg/(msK$^{\frac{1}{2}}$) and $T_S = 170.672$ K.

The linearization is obtained by a first order Taylor expansion:

$$\mu = \underbrace{\mu(\overline{T})}_{\overline{\mu}} + \frac{\partial\mu}{\partial T}\Big|_{\overline{T}} \underbrace{T-\overline{T}}_{T'}$$

$$\mu' = \mu - \overline{\mu} = \frac{\partial}{\partial T}\left[\frac{A_S\sqrt{T}}{1+\frac{T_S}{T}}\right]\Big|_{\overline{T}} T'$$

$$\mu' = \overline{\mu}\frac{\overline{T}+3T_S}{2(\overline{T}+T_S)}\frac{T'}{\overline{T}} \tag{2.8}$$

Note, that in eq. (2.8) the linearized viscosity perturbation μ' is a function of the perturbation value for temperature T', which is not part of $\boldsymbol{\varphi'}$. Using the ideal gas law, T' can be substituted by variables of $\boldsymbol{\varphi'}$. The ideal gas law for mixtures reads:

$$p \;=\; \rho\,\mathscr{R}\,T\sum_i \frac{Y_k}{W_k} \tag{2.9}$$

As only premixed combustion is considered, the ideal gas constant remains constant at $\mathscr{R} = 8.314$ J/(mol K). The first order Taylor polynomial for the equation above - interpreted as $p \;=\; f(\rho,\; T,\; Y_i)$ - reads:

$$p \;= \overline{p} + \frac{\partial p}{\partial\rho}\Big|_{\overline{\varphi}}(\rho-\overline{\rho}) + \frac{\partial p}{\partial T}\Big|_{\overline{\varphi}}(T-\overline{T}) + \frac{\partial p}{\partial Y_k}\Big|_{\overline{\varphi}}(Y_k-\overline{Y_k})$$

$$p-\overline{p} = \Big(\mathscr{R}\overline{T}\sum_k\frac{\overline{Y}_k}{W_k}\Big)\rho' + \Big(\overline{\rho}\mathscr{R}\sum_k\frac{\overline{Y}_k}{W_k}\Big)T' + \Big(\overline{\rho}\mathscr{R}\sum_k\frac{1}{W_k}\Big)Y_k'$$

$$p' = \Big(\overline{\rho}\mathscr{R}\overline{T}\sum_k\frac{\overline{Y}_k}{W_k}\Big)\frac{\rho'}{\overline{\rho}} + \Big(\overline{\rho}\mathscr{R}\overline{T}\sum_k\frac{\overline{Y}_k}{W_k}\Big)\frac{T'}{\overline{T}} + \Big(\overline{\rho}\mathscr{R}\overline{T}\sum_k\frac{\overline{Y}_k}{W_k}\Big)\frac{Y_i'}{\overline{Y}_k}$$

After dividing by $\overline{p} = \overline{\rho}\mathscr{R}\overline{T}\sum_k\frac{\overline{Y}_k}{W_k}$ and replacing $\frac{Y_k'}{\overline{Y}_k} = \frac{\sum_k Y_k'/W_k}{\sum_k\overline{Y}_k/W_k} = \overline{W}\sum_k\frac{Y_k'}{W_K}$, the linearized ideal gas law (LIGL) is obtained as:

$$\frac{p'}{\overline{p}} = \frac{\rho'}{\overline{\rho}} + \frac{T'}{\overline{T}} + \overline{W}\sum_k\frac{Y_k'}{W_k} \tag{2.10}$$

Thus, the perturbation viscosity can be expressed as:

$$\mu' = \overline{\mu}\frac{\overline{T}+3T_S}{2(\overline{T}+T_S)}\left(\frac{p'}{\overline{p}} - \frac{\rho'}{\overline{\rho}} - \overline{W}\sum_k\frac{Y_k'}{W_k}\right) \tag{2.11}$$

2.2.3 Species equation

By the same treatment (replace $\boldsymbol{\varphi}$ by $\overline{\boldsymbol{\varphi}}$ and $\boldsymbol{\varphi}'$, then apply MVP and neglect HO terms), the conservation of species k is obtained as:

$$\begin{aligned}\frac{\partial \rho' \overline{Y}_k}{\partial t} + \frac{\partial \overline{\rho} Y_k'}{\partial t} + \frac{\partial \overline{\rho u} Y_k'}{\partial x} + \frac{\partial \overline{\rho} u' \overline{Y}_k}{\partial x} + \frac{\partial \rho' \overline{u} \overline{Y}_k}{\partial x} + \frac{\partial \overline{\rho v} Y_k'}{\partial y} + \frac{\partial \overline{\rho} v' \overline{Y}_k}{\partial y} + \frac{\partial \rho' \overline{v} \overline{Y}_k}{\partial y} = \\ \frac{\partial}{\partial x}\left(\overline{D}_k \frac{\partial Y_k'}{\partial x}\right) + \frac{\partial}{\partial x}\left(D_k' \frac{\partial \overline{Y}_k}{\partial x}\right) + \frac{\partial}{\partial y}\left(\overline{D}_k \frac{\partial Y_k'}{\partial y}\right) + \frac{\partial}{\partial y}\left(D_k' \frac{\partial \overline{Y}_k}{\partial y}\right) + \dot{\omega}_k{}'\end{aligned} \tag{2.12}$$

Modeling of diffusion coefficients D_k

By the assumption on the Lewis number, Le = 1 (cf. [3, p. 39] and [18, p. 411]), the thermal diffusivity can be expressed as:

$$\mathrm{Le} = \frac{\mathrm{Sc}}{\mathrm{Pr}} = \frac{\alpha}{D_k} = 1 \quad \Longleftrightarrow \quad \alpha = D_k$$

with the Schmidt number Sc and Prandtl number Pr. This relation shows that thermal and species mass diffusion are ruled by the same correlations. Consequently, mass diffusivity is the same for all species and is written without index k further on. The linearization of α is shown with the energy equation in the next section.

Modeling of premixed flame combustion with one-step chemistry

The linearization of the reaction term $\dot{\omega}_k$ is conducted differently from the previous terms, as it depends on the chemical reaction. The general form of a chemical reaction is

$$\sum_{k=1}^{K} \nu_{kn}' \mathscr{M}_k \rightleftharpoons \sum_{k=1}^{K} \nu_{kn}'' \mathscr{M}_k \tag{2.13}$$

with the k-th chemical species symbol $\mathscr{M}_k$, and the n-th reaction stoichiometric coefficients for reactants (ν_{kn}') and products (ν_{kn}''). The reaction rate $\dot{\omega}_k$ is formulated

$$\dot{\omega}_k = \sum_{n=1}^{N} \dot{\omega}_{kn} = W_k \sum_{n=1}^{N} \nu_{kn} \mathscr{Q}_n \tag{2.14}$$

$$\text{with} \qquad \frac{\dot{\omega}_{kn}}{W_k \nu_{kn}} = \mathscr{Q}_n \qquad \text{and} \qquad \nu_{kn} = \nu_{kn}'' - \nu_{kn}'$$

The rate of progress of the n-th reaction $\mathscr{Q}_n$ is

$$\mathscr{Q}_n = K_{f,n} \prod_{k=1}^{K} [X_k]^{\nu_{kn}'} - K_{r,n} \prod_{k=1}^{K} [X_k]^{\nu_{kn}''} \tag{2.15}$$

The forward rate K_{fn} and backward rate K_{rn} are modelled by an Arrhenius ansatz:

$$K_{f,n} = A_{fn}\left(\frac{T}{T_{ref}}\right)^{\beta}\exp\left(-\frac{E_a}{RT}\right) \tag{2.16}$$

where A_{fn} is a pre-exponential factor, β_n the temperature exponent, T_{ref} a reference temperature. The activation energy is formulated $E_a = RT_a$ where T_a is the activation temperature.

We consider methane combustion a one-step mechanism, as proposed by Westbrook and Dryer [19]. Now, the chemical reaction (cf. eq. (2.13)) reads:

$$CH_4 + 2O_2 \rightarrow CO_2 + 2H_2O \tag{2.17}$$

Further simplifications are the absence of a reverse reaction ($K_{rn} = 0$) and setting β to zero. Thereby equations (2.15) and (2.16) simplify to

$$\mathcal{Q}_n = A\exp\left(-\frac{T_a}{T}\right)[O_2]^a[CH_4]^b \tag{2.18}$$

which is shortened to $\mathcal{Q}$ for readability of further expressions. The exponents a and b are taken from [19, p. 36f.] to be 1.3 and 0.2 respectively.

Now, the molar concentrations are substituted by $[X_i] = \rho\frac{Y_i}{W_i}$:

$$\begin{aligned}\mathcal{Q} &= A\exp\left(-\frac{T_a}{T}\right)\left(\rho\frac{Y_{O_2}}{W_{O_2}}\right)^a\left(\rho\frac{Y_{CH_4}}{W_{CH_4}}\right)^b \\ &= A\exp\left(-\frac{T_a}{T}\right)\rho^{a+b}\frac{1}{W_{O_2}^a W_{CH_4}^b}(Y_{O_2})^a(Y_{CH_4})^b\end{aligned} \tag{2.19}$$

The linearization of eq. (2.19) is given by:

$$\mathcal{Q} = \overline{\mathcal{Q}} + \frac{\partial\mathcal{Q}}{\partial\rho}\Big|_{\overline{\boldsymbol{\varphi}}}\underbrace{(\rho-\overline{\rho})}_{\rho'} + \frac{\partial\mathcal{Q}}{\partial T}\Big|_{\overline{\boldsymbol{\varphi}}}\underbrace{(T-\overline{T})}_{T'} + \sum_i \frac{\partial\mathcal{Q}}{\partial Y_i}\Big|_{\overline{\boldsymbol{\varphi}}}\underbrace{(Y_i-\overline{Y}_k)}_{Y_i'}$$

with

$$\begin{aligned}\frac{\partial\mathcal{Q}}{\partial\rho}\Big|_{\overline{\boldsymbol{\varphi}}} &= \frac{a+b}{\overline{\rho}}\overline{\mathcal{Q}} \\ \frac{\partial\mathcal{Q}}{\partial T}\Big|_{\overline{\boldsymbol{\varphi}}} &= \frac{T_a}{\overline{T}}\frac{1}{\overline{T}}\overline{\mathcal{Q}} \\ \frac{\partial\mathcal{Q}}{\partial Y_{O_2}}\Big|_{\overline{\boldsymbol{\varphi}}} &= \frac{a}{\overline{Y}_{O_2}}\overline{\mathcal{Q}} \\ \frac{\partial\mathcal{Q}}{\partial Y_{CH_4}}\Big|_{\overline{\boldsymbol{\varphi}}} &= \frac{b}{\overline{Y}_{CH_4}}\overline{\mathcal{Q}}\end{aligned}$$

Using $\mathscr{Q}-\overline{\mathscr{Q}}=\mathscr{Q}'$ and substituting $\frac{T'}{\overline{T}}$ from eq. (2.10), the rate of progress for reaction (2.17) is linearized as:

$$\frac{\mathscr{Q}'}{\overline{\mathscr{Q}}}=(a+b)\frac{\rho'}{\overline{\rho}}+\frac{T_a}{\overline{T}}\left(\frac{p'}{\overline{p}}-\frac{\rho'}{\overline{\rho}}-\overline{W}\sum_i\frac{Y_k'}{W_i}\right)+\frac{a}{\overline{Y}_{O_2}}Y_{O_2}'+\frac{b}{\overline{Y}_{CH_4}}Y_{CH_4}' \tag{2.20}$$

As $\overline{Y}_{CH_4}$ appears in the denominator of this equation, its minimum value is limited to avoid problems in numerical simulation: $\left(\overline{Y}_{CH_4}\right)_{\min}=10^{-4}\cdot\left(\overline{Y}_{CH_4}\right)_{\max}$.

The right hand side of equation (2.20) is from now on referred to as $f(\rho',p',Y_k')$. Inserting this relation into eq.(2.14) yields:

$$\frac{\dot{\omega}_k'}{\overline{\dot{\omega}}_k}=\frac{W_k\nu_{kn}\mathscr{Q}'}{W_k\nu_{kn}\overline{\mathscr{Q}}}=f(\rho',p',Y_k')\qquad\Rightarrow\qquad\dot{\omega}_k'=\overline{\dot{\omega}}_k\cdot f(\rho',p',Y_k')$$

and in the end we can formulate the reaction rate as

$$\dot{\omega}_k=\overline{\dot{\omega}}_k+\dot{\omega}_k'=\overline{\dot{\omega}}_k+\overline{\dot{\omega}}_k f(\rho',p',Y_k') \tag{2.21}$$

which has the same rate of progress for all species in this combustion process. Be reminded, that the mean reaction rates $\overline{\dot{\omega}}_k$ still contains stoichiometric coefficient ν_{kn} and molar weight W_k and are species specific!

2.2.4 Sensible enthalpy equation

Finally, the conservation law for sensible enthalpy reads in linearized form:

$$\begin{aligned}\frac{\partial}{\partial t}\left(\rho'\overline{h}+\overline{\rho}h'-p'\right)+\frac{\partial}{\partial x}\left(\overline{\rho}\,\overline{u}h'+\overline{\rho}u'\overline{h}+\rho'\overline{u}\,\overline{h}\right)+\frac{\partial}{\partial y}\left(\overline{\rho}\,\overline{v}h'+\overline{\rho}v'\overline{h}+\rho'\overline{v}\,\overline{h}\right)=\\ \overline{\dot{\omega}}_T\cdot f(\rho',p',Y_k')+\frac{\partial}{\partial x}\alpha'\frac{\partial\overline{h}}{\partial x}+\frac{\partial}{\partial x}\overline{\alpha}\frac{\partial h'}{\partial x}+\frac{\partial}{\partial y}\alpha'\frac{\partial\overline{h}}{\partial y}+\frac{\partial}{\partial y}\overline{\alpha}\frac{\partial h'}{\partial y}\end{aligned} \tag{2.22}$$

Modeling of heat release with one-step chemistry

The heat release term $\dot{\omega}_T$ can be formulated by the reaction rate ω_k as follows:

$$\dot{\omega}_T=-\sum_k\Delta h_{f,k}^0\omega_k=-\sum_k\left(\Delta h_{f,k}^0W_k\nu_{kn}\right)\mathscr{Q} \tag{2.23}$$

with $\Delta h_{f,k}^0$ as the standard enthalpy of formation for each species.

Now, we can express $\dot{\omega}_T$ as a linear function of $\mathscr{Q}$ similar to equation (2.20):

$$\frac{\dot{\omega}_T'}{\overline{\dot{\omega}}_T}=\frac{\mathscr{Q}'}{\overline{\mathscr{Q}}}=f(\rho',p',Y_k') \tag{2.24}$$

Therefore, it is linearized as:

$$\dot{\omega}_T=\left[\overline{\dot{\omega}}_T\right]+\overline{\dot{\omega}}_T\cdot f(\rho',p',Y_k') \tag{2.25}$$

Modeling of heat conductivity with Sutherland law

For the energy diffusion terms $\frac{\partial}{\partial x_i}\alpha\frac{\partial h}{\partial x_i}$, the linearization of the thermal diffusion coefficient α has to be considered. By assuming a constant Prandtl number Pr, the heat conductivity can be also expressed by the Sutherland law:

$$\alpha = \frac{\mu}{\mathrm{Pr}} = \frac{1}{\mathrm{Pr}}\frac{A_S\sqrt{T}}{1+\frac{T_S}{T}} \tag{2.26}$$

As air is the dominant mixture fraction and pressure perturbations are assumed to be comparatively small, a constant Pr is justifiable.

The linearization is obtained as:

$$\begin{aligned}
\alpha = \overline{\alpha} + \alpha' &= \alpha(\overline{T}) + \frac{\partial\alpha}{\partial T}\Big|_{\overline{T}}(T-\overline{T}) \\
\alpha' = \alpha - \overline{\alpha} &= \frac{1}{\mathrm{Pr}}\frac{\partial}{\partial T}\Big(\frac{A_S\sqrt{T}}{1+\frac{T_S}{T}}\Big)\Big|_{\overline{T}} \quad T' \\
&= \frac{1}{\mathrm{Pr}}\frac{A_S\sqrt{\overline{T}}}{1+\frac{T_S}{\overline{T}}}\frac{\overline{T}+3T_S}{2(\overline{T}+T_S)}\frac{T'}{\overline{T}}
\end{aligned}$$

$$\alpha' = \overline{\alpha}\frac{\overline{T}+3T_S}{2(\overline{T}+T_S)}\frac{T'}{\overline{T}} \tag{2.27}$$

Linearization of enthalpy h

As described in section 2.1, sensible enthalpy h is formulated with the heat capacity being a polynomial of 4th degree as suggested by Burcat [21]. Values for the polynomial factors $a_{n,k}$ are taken from [22].

The linearization of enthalpy then reads as follows:

$$\begin{aligned}
h = \quad & \overline{h} && + && h'_T && + && h'_Y \\
= \quad & h\big(\overline{T},\overline{Y}_k\big) && + && \frac{\partial h}{\partial T}\Big|_{\overline{T},\overline{Y}_k}\big(T-\overline{T}\big) && + && \frac{\partial h}{\partial Y_i}\Big|_{\overline{T},\overline{Y}_k}\big(Y_k-\overline{Y}_k\big)
\end{aligned}$$

with

$$h(\overline{T},\overline{Y}_k) = \int_{T_{\text{ref}}}^{\overline{T}} c_p(\tilde{T},\overline{Y}_k)d\tilde{T} = \underbrace{\sum_k R_k\Big[\sum_{n=0}^{4} a_{n,k}\frac{\overline{T}^{n+1}-T_{\text{ref}}^{n+1}}{n+1}\Big]\overline{Y}_k}_{\overline{h}}$$

$$\frac{\partial h}{\partial T}\Big|_{\overline{T},\overline{Y}_k}(T-\overline{T}) = \frac{\partial}{\partial T}\int_{T_{\text{ref}}}^{\overline{T}} c_p(\tilde{T},\overline{Y}_k)d\tilde{T}\;\; T' = \underbrace{\sum_k R_k\Big[\sum_{n=0}^{4} a_{n,k}\overline{T}^{n}\Big]\overline{Y}_k}_{\overline{c}_p}\;\; T'$$

$$\frac{\partial h}{\partial Y_k}\Big|_{\overline{T},\overline{Y}_k}(Y_k-\overline{Y}_k) = \frac{\partial}{\partial Y_k}\int_{T_{\text{ref}}}^{\overline{T}} c_p(\tilde{T},\overline{Y}_k)d\tilde{T}\;\; Y_k' = \sum_k \underbrace{\Big[R_k\Big[\sum_{n=0}^{4} a_{n,k}\frac{\overline{T}^{n+1}-T_{\text{ref}}^{n+1}}{n+1}\Big]\Big]}_{\overline{h}_{Y_i}} Y_k'$$

Hence, linearized sensible enthalpy is obtained as:

$$h' = h'_T + h'_Y = \overline{c}_p T' + \sum_k \overline{h}_{Y_k} Y'_k \tag{2.28}$$

3 Reduction of Independent Variables

In the previous chapter, the LRF equations are written as partial differential equations (PDE) of the field variable vector $\boldsymbol{\varphi}$. The vector $\boldsymbol{\varphi}'$ in this form has 8 entries: the flow properties ρ', u', v' and p', as well as 4 out of 5 occurring species mass fractions Y'_{CH_4}, Y'_{O_2}, Y'_{N_2}, Y'_{CO_2} and Y'_{H_2O}[1].

In the following chapter a different formulation is shown, that expresses the five Y_i by only two variables: nitrogen's mass fraction and methane's mass fraction. The choice for these two is made, because nitrogen (N_2) is not taking part in the global one-step reaction and thus represents the transport of equivalence ration perturbations through the domain. Methane (CH_4) on the other hand is completely consummated during combustion and can thus be used to describe the generation of carbon dioxide (CO_2) and water (H_2O).

Other possible choices could be the equivalence ratio ϕ or a progress variable ξ, for both of which definitions are given later on in the chapter.

3.1 Species conservation for nitrogen

In order to describe how perturbations are transported through the domain, the species equation for nitrogen N_2 is very useful. Since N_2 does not react in the flame, its species equation is decoupled from the remaining PDE. Otherwise mixture fraction perturbations could be tracked by transporting a small fraction of argon Ar. To improve readability, Y_{N_2} is renamed Z from now on.

The linearized conservation equation for nitrogen's mass fraction reads:

$$\begin{aligned}\frac{\partial \rho' \overline{Z}}{\partial t} + \frac{\partial \overline{\rho} Z'}{\partial t} + \frac{\partial \overline{\rho u} Z'}{\partial x} + \frac{\partial \overline{\rho} u' \overline{Z}}{\partial x} + \frac{\partial \rho' \overline{u} \overline{Z}}{\partial x} + \frac{\partial \overline{\rho v} Z'}{\partial y} + \frac{\partial \overline{\rho} v' \overline{Z}}{\partial y} + \frac{\partial \rho' \overline{v} \overline{Z}}{\partial y} = \\ \frac{\partial}{\partial x}\left(\overline{D}\frac{\partial Z'}{\partial x}\right) + \frac{\partial}{\partial x}\left(D'\frac{\partial \overline{Z}}{\partial x}\right) + \frac{\partial}{\partial y}\left(\overline{D}\frac{\partial Z'}{\partial y}\right) + \frac{\partial}{\partial y}\left(D'\frac{\partial \overline{Z}}{\partial y}\right)\end{aligned} \tag{3.1}$$

Note, that the reaction rate $\dot{\omega}'_Z$ is already left out. As nitrogen doesn't react, its mean field $\overline{Z}$ will remain constant over the whole domain and its gradients are therefore zero.

The next step to simplify eq. (3.1) comes from multiplying the linearized continuity equation (2.4) with $\overline{Z}$:

[1] As the sum of mass fractions must be always 1, it is not necessary to solve conservation equations for all species. Alternatively, one could also omit the continuity equation and solve all species equations instead.

$$\frac{\partial \rho' \overline{Z}}{\partial t} + \frac{\partial \rho' \overline{u} \overline{Z}}{\partial x} + \frac{\partial \overline{\rho} u' \overline{Z}}{\partial x} + \frac{\partial \rho' \overline{v} \overline{Z}}{\partial y} + \frac{\partial \overline{\rho} v' \overline{Z}}{\partial y} = 0 \tag{3.2}$$

After inserting equation (3.2) and neglecting all gradients of $\overline{Z}$, equation (3.1) becomes:

$$\frac{\partial \overline{\rho} Z'}{\partial t} + \frac{\partial \overline{\rho u} Z'}{\partial x} + \frac{\partial \overline{\rho v} Z'}{\partial y} = \frac{\partial}{\partial x}\left(\overline{D}\frac{\partial Z'}{\partial x}\right) + \frac{\partial}{\partial y}\left(\overline{D}\frac{\partial Z'}{\partial y}\right) \tag{3.3}$$

Applying partial differentiation on the left-hand side, the mean value form of the continuity equation (2.1) appears and can be cancelled out as well:

$$\frac{\partial \overline{\rho} Z'}{\partial t} + \frac{\partial \overline{\rho u} Z'}{\partial x} + \frac{\partial \overline{\rho v} Z'}{\partial y} = \overline{\rho}\frac{\partial Z'}{\partial t} + \overline{\rho u}\frac{\partial Z'}{\partial x} + \overline{\rho v}\frac{\partial Z'}{\partial y} + Z' \underbrace{\left(\frac{\partial \overline{\rho}}{\partial t} + \frac{\partial \overline{\rho u}}{\partial x} + \frac{\partial \overline{\rho v}}{\partial y}\right)}_{=0, \text{ cf. MVP}}$$

The final decoupled equation is written as:

$$\overline{\rho}\frac{\partial Z'}{\partial t} + \overline{\rho u}\frac{\partial Z'}{\partial x} + \overline{\rho v}\frac{\partial Z'}{\partial y} = \frac{\partial}{\partial x}\left(\overline{D}\frac{\partial Z'}{\partial x}\right) + \frac{\partial}{\partial y}\left(\overline{D}\frac{\partial Z'}{\partial y}\right) \tag{3.4}$$

This decoupled PDE for nitrogen (3.4) now contains no entries from the flow variable vector $\boldsymbol{\varphi'}$ other than $Y'_{N_2} = Z'$, and can therefore be solved independently from the rest of the coupled system of equations.

3.2 Reformulation of variable vector $\boldsymbol{\varphi'}$

The expressions for is the reaction equation (cf. eq. (2.17)) for methane-air combustion rewritten as:

$$CH_4 + 2\underbrace{(O_2 + 3.76N_2)}_{\text{dry air}} \rightarrow CO_2 + 2H_2O + 7.52N_2 \tag{3.5}$$

In this formulation all species are included and their molar proportions known. These can be described by the following relations in order to shorten some expressions.

Composition of dry air

The ratio of mass fractions in dry air (at the inlet) is assumed fixed and called γ_{air}:

$$\gamma_{\text{air}} = \frac{Y_{O_2,\text{air}}}{Y_{N_2,\text{air}}} = \frac{X_{O_2} W_{O_2} \frac{1}{W}}{X_{N_2} W_{N_2} \frac{1}{W}} = \frac{1}{3.76}\frac{32\frac{g}{mol}}{28\frac{g}{mol}} = 0.304$$

This fixed mass fraction relation of nitrogen and oxygen before reaction will be used later on.

$$Y_{O_2,\text{air}} = \gamma_{\text{air}}\, Y_{N_2,\text{air}} \tag{3.6}$$

Equivalence ratio ϕ

The equivalence ratio ϕ describes the composition of fresh gases at the intake as:

$$\phi = \frac{\dot{m}_{\text{fuel}}/\dot{m}_{\text{oxidizer}}}{\left(\dot{m}_{\text{fuel}}/\dot{m}_{\text{oxidizer}}\right)_{\text{st}}} = s\frac{Y_{\text{fuel}}}{Y_{\text{oxidizer}}} = s\frac{Y_{CH_4}}{Y_{O_2}} \tag{3.7}$$

$$\text{with} \quad s = \frac{2W_{O_2}}{W_{CH_4}} = 4$$

The mass stoichiometric ratio s is constant, whilst ϕ changes with fuel inlet perturbations. For lean combustion the equivalence ratio takes values $\phi < 1$. That means, that there is not enough methane in the combustion chamber, to consume all available oxygen.

Figure 3.1 shows the case of stoichiometric combustion ($\phi = 1$) in 1D with typical developments of fuel and oxidizer mass fractions, temperature, reaction rate and progress variable ξ. An exemplary definition of ξ is given in Appendix B.

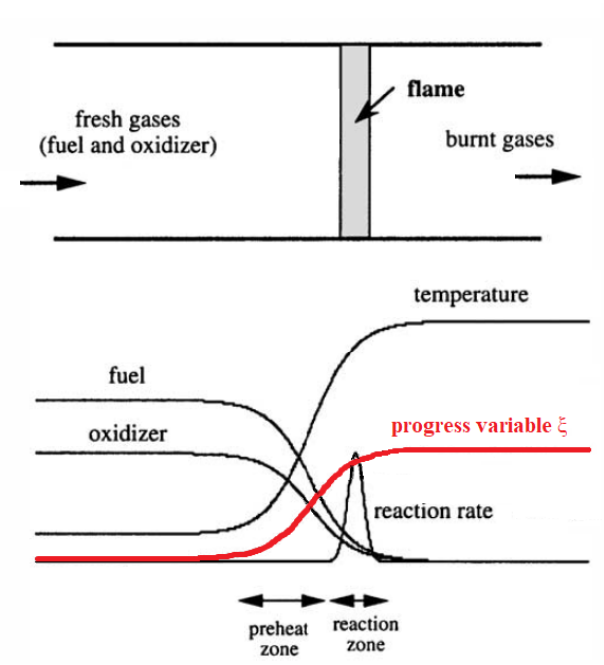

Figure 3.1: Laminar premixed flame in 1D at equivalence ratio $\phi = 1$. Figure modified from Veynante and Vervisch [1, p. 200]

φ' by Y' and Z'

In order to shorten expressions, the mass fraction for methane Y_{CH_4} is written as Y further on.

$$Y_{N_2} = Y_{N_2,0} \equiv Z \tag{3.8}$$

$$Y_{CH_4} = \underbrace{Y_{CH_4,nr}}_{\text{not yet reacted}} \equiv Y \tag{3.9}$$

Analytic expressions for the reduction of number of variables for mass fractions are deduced from eq. (3.5). The following equations for mass fractions of oxygen O_2, carbon dioxide CO_2 and water H_2O were developed together with supervisor Alexander Avdonin.

$$Y_{O_2} = \underbrace{Y_{O_2,0}}_{\text{initial oxygen}} - \underbrace{Y_{O_2,r}}_{\text{reacted}} = \gamma_{\text{air}} Z - s\,(Y_{CH_4,0} - Y) \tag{3.10}$$

$$Y_{CO_2} = \frac{W_{CO_2}}{W_{CH_4}} \underbrace{Y_{CH_4,r}}_{\text{already reacted}} = \frac{W_{CO_2}}{W_{CH_4}} (Y_{CH_4,0} - Y) \tag{3.11}$$

$$Y_{H_2O} = \frac{2\,W_{H_2O}}{W_{CH_4}} \underbrace{Y_{CH_4,r}}_{\text{already reacted}} = \frac{2\,W_{H_2O}}{W_{CH_4}} (Y_{CH_4,0} - Y) \tag{3.12}$$

Here, $Y_{CH_4,0}$ denotes the total mass fraction of methane flowing into the domain, it is available before reaction in the flame. $Y_{CH_4,0}$ can be expressed by Z from the constraint 'the sum of all mass fractions must be equal 1':

$$Y_{CH_4,0} = 1 - Y_{O_2,0} - Y_{N_2,0} = 1 - (1 + \gamma_{\text{air}}) Z$$

The linearized perturbations are obtained as:

$$Y'_{N_2} = Z' \tag{3.13}$$

$$Y'_{CH_4} = Y' \tag{3.14}$$

$$Y'_{O_2} = \gamma_{\text{air}}\, Z' + s\left((1 + \gamma_{\text{air}}) Z' + Y'\right) \tag{3.15}$$

$$Y'_{CO_2} = -\frac{W_{CO_2}}{W_{CH_4}} \left((1 + \gamma_{\text{air}}) Z' + Y'\right) \tag{3.16}$$

$$Y'_{H_2O} = -\frac{2\,W_{H_2O}}{W_{CH_4}} \left((1 + \gamma_{\text{air}}) Z' + Y'\right) \tag{3.17}$$

An analytic examination of the relations in eqns. (3.8)-(3.12) and (3.13)-(3.17) is given in appendix B, where it it shown that the sum of all mass fractions adds up to 1 for total values and zero for pertubations respectively.

Applying the formulations in eqn. (3.13)-(3.17), the sum of mass fraction perturbations becomes

$$\begin{aligned}\sum_i \frac{Y_k'}{W_i} = &\underbrace{\left(\frac{1}{W_{CH_4}} + \frac{s}{W_{O_2}} - \frac{W_{CO_2}}{W_{CH_4}W_{CO_2}} - \frac{2\,W_{H_2O}}{W_{CH_4}W_{H_2O}}\right)}_{=\frac{1}{W_{CH_4}}(1+2-1-2)=0} Y' \\ &+\left(\frac{\gamma_{\text{air}}}{W_{O_2}} \underbrace{+\frac{2\,s}{W_{CH_4}}(1+\gamma_{\text{air}}) - \frac{W_{CO_2}}{W_{CH_4}W_{CO_2}}(1+\gamma_{\text{air}}) - \frac{2\,W_{H_2O}}{W_{CH_4}W_{H_2O}}(1+\gamma_{\text{air}})}_{=\frac{1}{W_{CH_4}}(2-1-2)(1+\gamma_{\text{air}})=-\frac{1+\gamma_{\text{air}}}{W_{CH_4}}} + \frac{1}{W_{N_2}}\right) Z'\end{aligned}$$

and is just an expression of Z'. This sum is used in the linearized ideal gas law (LIGL) as given by eq. (2.10) and the term $\overline{W}\sum_i \frac{Y_k'}{W_i}$ simplifies to :

$$\overline{W}\sum_i \frac{Y_k'}{W_i} = \underbrace{\overline{W}\left(\frac{\gamma_{\text{air}}}{W_{O_2}} - \frac{1+\gamma_{\text{air}}}{W_{CH_4}} + \frac{1}{W_{N_2}}\right)}_{=k_{\sum Y'}} Z' = k_{\sum Y'}\, Z'. \tag{3.18}$$

Applying the formulations in eqns. (3.17)-(3.17) and (3.18) to eqns. (2.11), (2.21), (2.24) and (2.27), all can be expressed as functions of a new variable vector $\boldsymbol{\varphi}'_{YZ}$.

$$\boldsymbol{\varphi}'_{YZ} = \begin{pmatrix} \rho' \\ u' \\ v' \\ p' \\ Y' \\ Z' \end{pmatrix} \tag{3.19}$$

Importantly, eq. (2.20) can now be written as:

$$\begin{aligned} f(\boldsymbol{\varphi}'_{reac}) = (a+b)\frac{\rho'}{\overline{\rho}} + \frac{T_a}{\overline{T}}\left(\frac{p'}{\overline{p}} - \frac{\rho'}{\overline{\rho}} - k_{\sum Y'}\, Z'\right) \\ + \frac{a}{\overline{Y}_{O_2}}\left(\gamma_{\text{air}}\, Z' + s\left((1+\gamma_{\text{air}})Z' + Y'\right)\right) + \frac{b}{\overline{Y}_{CH_4}}\, Y' \end{aligned} \tag{3.20}$$

The term h'_Y from eq.(2.28) in this formulation reads:

$$\begin{aligned} h'_Y = &\left(\overline{h}_{CH_4} + s\,\overline{h}_{O_2} - \frac{\overline{h}_{CO_2}\,W_{CO_2}}{W_{CH_4}} - \frac{2\,\overline{h}_{H_2O}\,W_{H_2O}}{W_{CH_4}}\right) Y' \\ &+\left(\overline{h}_{O_2}\left(\gamma_{\text{air}} + s\left(1+\gamma_{\text{air}}\right)\right) - \frac{\overline{h}_{CO_2}\,W_{CO_2}}{W_{CH_4}}\left(1+\gamma_{\text{air}}\right)\right. \\ &\left. - \frac{2\,\overline{h}_{H_2O}\,W_{H_2O}}{W_{CH_4}}\left(1+\gamma_{\text{air}}\right) + \overline{h}_{N_2}\right) \quad Z' \end{aligned} \tag{3.21}$$

Applying the formulations from this chapter makes the solution of the PDEs faster, as the original variable vector $\boldsymbol{\varphi}'$ is shortened from 8 to 6 entries in $\boldsymbol{\varphi}'_{YZ}$. Consequently, the numerical problem size is also reduced, making the numerical solution less expensive in terms of computation time and storage demand. With the decoupling of the species equation for Z, only 5 indepedent variables are coupled and have to be solved for simultaneously.

4 The Discontinuous Galerkin Method

The discontinuous Galerkin Finite Element Method (DG-FEM) is commonly described as a "hybrid method" between classical finite element and finite volume approaches. Typical advantages of FEM over FVM are 'the straight-forward extendibility to higher order schemes (pFEM) and the applicability to unstructured meshes' [23, p.3]. The uses in standard FEM, however, causes numerical instability, due to the discretezation of the convective terms. Recently the discontinuous Galerkin method has shown to be a suitable numerical approach on convection dominated problems. Its discretization of linear and non-linear PDEs yields stable schemes with high accuracy and high convergence potential[23, p.4].

The use of FEM requires an integral formulation of the PDE (strong form), that is multiplied by test functions (giving the weak form), and then solved for each discrete element separately (Galerkin form). For the DG-FEM these test functions do not have to be point-wise equal on neighboring element nodes, but can have steps between each element. These jumps constitute a Riemann problem at each element face and are balanced by fluxes between elements, a modelling approach typical for FVM.

The deduction of the DG-form for LRF equations is first shown for mass conservation in detail. Later on, all other LNSE are listed as used in DG-FEM.

4.1 DG-FEM of Mass Conservation

The strong form of the linearized mass equation (2.4) for the computational domain Ω reads:

$$\int_\Omega \left[\frac{\partial \rho'}{\partial t} + \frac{\partial \rho' \overline{u}}{\partial x} + \frac{\partial \overline{\rho} u'}{\partial x} + \frac{\partial \rho' \overline{v}}{\partial y} + \frac{\partial \overline{\rho} v'}{\partial y} \right] d\Omega = 0 \tag{4.1}$$

Multiplying this equation with an ansatz function l_{φ_i} for the respective variable, yields the weak form. For the continuity equation, this ansatz function is l_ρ:

$$\int_\Omega l_\rho \left[\frac{\partial \rho'}{\partial t} + \frac{\partial \rho' \overline{u}}{\partial x} + \frac{\partial \overline{\rho} u'}{\partial x} + \frac{\partial \rho' \overline{v}}{\partial y} + \frac{\partial \overline{\rho} v'}{\partial y} \right] d\Omega = 0 \tag{4.2}$$

Now, equation (4.2) is reformulated on element level Ω_e and the convective term solved by partial integration:

$$\begin{aligned} \int_{\Omega_e} l_\rho \frac{\partial \rho'}{\partial t} d\Omega_e - \int_{\Omega_e} \frac{\partial}{\partial x} \left[l_\rho (\rho' \overline{u} + \overline{\rho} u') \right] + \frac{\partial}{\partial y} \left[l_\rho (\rho' \overline{v} + \overline{\rho} v') \right] d\Omega_e \\ + \int_{\Omega_e} \frac{\partial l_\rho}{\partial x} \left(\rho' \overline{u} + \overline{\rho} u' \right) + \frac{\partial l_\rho}{\partial y} \left(\rho' \overline{v} + \overline{\rho} v' \right) d\Omega_e = 0 \end{aligned}$$

To formulate the final equation, the third term is transformed by applying Gauss's theorem.

$$\int_{\Omega_e} l_\rho \frac{\partial \rho'}{\partial t} - \left[\frac{\partial l_\rho}{\partial x}\left(\rho'\overline{u} + \overline{\rho}u'\right) + \frac{\partial l_\rho}{\partial y}\left(\rho'\overline{v} + \overline{\rho}v'\right) \right] d\Omega_e + \int_{\Gamma_e} l_\rho \underbrace{\left(\rho'\overline{u} + \overline{\rho}u'\right)n_x}_{\substack{\text{normal flux in x-direction} \\ f_{\rho,n_x}}} + l_\rho \underbrace{\left(\rho'\overline{v} + \overline{\rho}v'\right)n_y}_{\substack{\text{normal flux in y-direction} \\ f_{\rho,n_y}}} d\Gamma_e = 0 \tag{4.3}$$

Here, Γ_e denotes the element boundaries and n_i the element boundary's normal vector. The flux terms over the element boundaries f_{ρ,n_i}, which solve the local Riemann problem, are calculated by the local Lax-Friedrichs flux:

$$f_{\rho,n_i}^{lLF} = \frac{f_{\rho,n_i}(\Omega_e) + f_{\rho,n_i}(\Omega_{e+1})}{2} + \frac{C}{2}\left(\rho'(\Omega_e) - \rho'(\Omega_{e+1})\right) \tag{4.4}$$

where indices e and $e+1$ denote the current, and the neighboring element respectively. The constant C is based on the characteristic wave speed:

$$C = \max_{\Omega_e,\Omega_{e+1}} \overline{c} + |\overline{u}_i n_i| \qquad \text{with} \qquad \overline{c} = \sqrt{\kappa \frac{\overline{\rho}}{\overline{p}}}$$

4.2 DG-FEM of LRF

In general, the LRF equations can be written in short as

$$\frac{\partial \varphi'_i}{\partial t} + \frac{\partial \Psi'_j}{\partial x_j} = S'_{\varphi_i} \tag{4.5}$$

By the same approach as used above, the general DG-FEM formulation on element level reads:

$$\underbrace{\int_{\Omega_e} l_{\varphi_i} \underbrace{\frac{\partial \varphi'}{\partial t}}_{\substack{\text{transient change in} \\ \text{transport variable}}} + \frac{\partial l_{\varphi_i}}{\partial x_j}\Big(\underbrace{\Psi'_j}_{\text{flux}} - \int \underbrace{S'_{\varphi_i}}_{\text{sum of forces}} dx_i \Big) d\Omega_e}_{\text{change in cell volume}} \underbrace{- \int_{\Gamma_e} l_{\varphi_i}\left(\Psi'_j - \int S'_{\varphi_i} dx_i\right) n_{x_j} d\Gamma_e}_{\substack{\text{flux over cell boundaries} \\ f_{\varphi_i,n_i}}} = 0 \tag{4.6}$$

For LRF the transported variables φ', fluxes Ψ'_j, and source terms S'_{φ_i} are listed in table 4.1.

	φ'	Ψ'_j	S'_{φ_i}
Mass	ρ'	$\rho'\overline{u_j} + \overline{\rho}u'_j$	0
Momentum	$\rho'\overline{u_i} + \overline{\rho}u'_i$	$\rho'\overline{u_i u_j} + \overline{\rho}u'_i\overline{u_j} + \overline{\rho u_i}u'_j + \frac{\partial p'}{\partial x_i} - \frac{\partial \tau'_{i,j}}{\partial x_j}$	0
Species Y	$\rho'\overline{Y} + \overline{\rho}Y'$	$\rho'\overline{Y}\overline{u_j} + \overline{\rho}Y'\overline{u_j} + \overline{\rho}\overline{Y}u'_j - \frac{\partial}{\partial x_i}(D'\frac{\partial \overline{Y}}{\partial x_i} + \overline{D}\frac{\partial Y'}{\partial x_i})$	$\dot{\omega}'_Y$
Species Z	$\overline{\rho}Z'$	$\overline{\rho u_j}Z' - \frac{\partial}{\partial x_i}(\overline{D}\frac{\partial Z'}{\partial x_i})$	0
Sensible enthalpy	$\rho'\overline{h} + \overline{\rho}h' - p'$	$\rho'\overline{u_j}\overline{h} + \overline{\rho}u'_j\overline{h} + \overline{\rho u_j}h' - \frac{\partial}{\partial x_i}(\overline{\alpha}\frac{\partial h'}{\partial x_i} + \alpha'\frac{\partial \overline{h}}{\partial x_i})$	$\dot{\omega}'_T$

Table 4.1: Transport variable φ', Flux term Ψ'_j and Source terms S'_{φ_i} for LRF

Note, that the force terms in eq. (4.6) mostly include derivatives $\frac{\partial}{\partial x}$, which cancel out the integral from partial integration similar to the flux terms. In the energy and species conservation equations however, heat release and reaction rate would have to be integrated and are therefore excluded from partial integration.

The fluxes over the element boundaries f_{φ_i,n_i} are calculated by the local Lax-Friedrichs flux

$$f^{lLF}_{\varphi_i,n_i} = \frac{f_{\varphi_i,n_i}(\Omega_e) + f_{\varphi_i,n_i}(\Omega_{e+1})}{2} + \frac{C}{2}\left(\varphi'_i(\Omega_e) - \varphi'_i(\Omega_{e+1})\right) \tag{4.7}$$

with the constant C being

$$C = \max_{\Omega_e,\Omega_{e+1}} \overline{c} + |\overline{u}_i n_i| \,, \qquad \overline{c} = \sqrt{\kappa\frac{\overline{\rho}}{\overline{p}}}$$

The full formulations for the x- and y-Momentum, the Species i, and the Energy equations are shown in Appendix C.

4.3 Flame frequency response calculation

In order to calculate the flame frequency response, the following discretized system of linear PDEs has to be solved:

$$\underline{\underline{\mathrm{E}}}\,\dot{\boldsymbol{\varphi}}' = \underline{\underline{\mathrm{K}}}\,\boldsymbol{\varphi}' + \boldsymbol{l} \tag{4.8}$$

where $\underline{\underline{\mathrm{E}}}$ is the mass matrix, $\underline{\underline{\mathrm{K}}}$ the stiffness matrix and $\boldsymbol{l}$ the load vector. For each frequency f the forced flame response is calculated with the ansatz function

$$\dot{\boldsymbol{\varphi}}' = \widehat{\boldsymbol{\varphi}}\, e^{i\,2\pi f t}. \tag{4.9}$$

Inserting eq. (4.9) into (4.8) yields the equation for the linearized fields:

$$i\,2\pi f \underline{\underline{\mathrm{E}}}\ \widehat{\boldsymbol{\varphi}} = \underline{\underline{\mathrm{K}}}\,\widehat{\boldsymbol{\varphi}} + \widehat{\boldsymbol{l}} \tag{4.10}$$

with the solution in frequency domain:

$$\widehat{\boldsymbol{\varphi}} = (i\,2\pi f\ \underline{\underline{\mathrm{E}}} - \underline{\underline{\mathrm{K}}})^{-1}\,\widehat{\boldsymbol{l}} \tag{4.11}$$

For the forced response of the linearized field $\widehat{\boldsymbol{\varphi}'}$, the inverse $(i\,2\pi f\ \underline{\underline{\mathrm{E}}} - \underline{\underline{\mathrm{K}}})^{-1}$ is computed in COMSOL by the direct solver MUMPS (MUltifrontal Massively Parallel sparse direct Solver). Simulation procedure is to first solve the decoupled Z-equation (3.4) independently on a band of frequencies, and then use the result as an input to solve the remainder of the LRF equations.

For larger problems, the use of an iterative method or cluster computation should be considered. From the linearized fields the heat release fluctuations can be computed using an integration matrix $\underline{\underline{\mathrm{B}}}$:

$$\widehat{\dot{Q}} = \underline{\underline{\mathrm{B}}}\,\widehat{\boldsymbol{\varphi}} \tag{4.12}$$

In this thesis the frequency response to equivalence ratio perturbations F_ϕ is defined by eq. (1.2), while the LRF solver computes it with respect to methane mass fraction perturbations $Y'/\overline{Y}$. Therefore, a correction factor has to be introduced in the post-processing. Its deduction is shown in Appendix D. This correction slightly lowers the gain values, but does not affect the phase.

5 Study of laminar premixed flames

The previously introduced LRF method is now applied to compute the flame responses to equivalence perturbations for laminar premixed flames. These types of flame can be seen in Bunsen burners or as a single flame in a multiple slit burner configuration.

The premixed flame setup is investigated under two boundary conditions. One yields an attached flame due to adiabatic boundary conditions on the slit wall, whereas for a constant temperature wall a lifted flame is obtained.

Also, two versions of the LRF solver are applied for the solution. In order to see if there is a trade-off between accuracy and computation time for the reduced model, the LRF solver with all species equations is also run. Results from the former are denoted 'LRF-YZ' and from the latter 'LRF-Full'.

At the end, we investigate the influence of mass fraction perturbations in the linearized ideal gas law and in enthalpy perturbations.

5.1 Numerical Setup in COMSOL

Geometry

The setup under investigation is inspired by the configuration described by Kornilov et al. [2] in fig. 5.1. Taking advantage of the geometric symmetries in the slit Bunsen-type burner, just half a slit is examined (as shown in fig. 5.2) in order to keep computational costs low.

For our geometry, the slit width d and distance l are d = 2mm and l = 3mm. The inflow and outflow lengths are 5 mm and 8 mm respectively. The slit sheet depth is 1 mm. Note, that only half the transversal lengths are depicted in fig. 5.2.

As the goal is to examine the possibility to replace DNS/LES identification of the flame response by the LRF solver, numerical results of this thesis will be compared to FRF intentified from OpenFOAM LES of exactly the same geometry. Also, the mean fields, which are not calculated by the LNSE, are taken from OpenFOAM simulation.

Meshing

The discretization and simulation is performed on a uniform mesh of 21100 quadratic plane elements, that each have a side length of $\Delta x = 40$ μm.

Element size in OpenFOAM (for the computation of the reference FRF with LES) is $\Delta x = 25$ μm, giving 53600 square cells. Avdonin et al. [14] tested mesh sizes of $\Delta x = 50$ μm and 40 μm. They show that the mesh with $\Delta x = 40$ μm yields similar results as the finer one with 25 μm, a strong hint of mesh convergence.

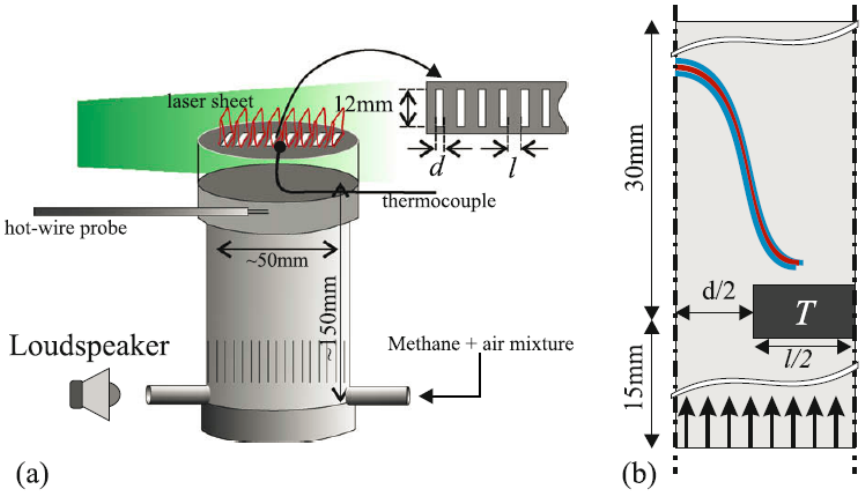

Figure 5.1: Combustion and flame model for the study: (a) Experimental and (b) deducted numerical setup. Figure modified from Kornilov et al. ([2, p. 1960]).

On every element linear test functions are solved, which gives 4 degrees of freedom (DOFs) per element for each independent variable in $\boldsymbol{\varphi'}_{YZ}$. The linear test functions' normalized forms can be seen in fig. 5.3. Thus, the model's total number of DOFs is:

$$\#\,\mathrm{DOFs}_{\mathrm{tot}} = \underbrace{4}_{\#\,\mathrm{DOFs\ per\ element}} \times \underbrace{6}_{\substack{\#\,\mathrm{independent\ variables} \\ [\rho', u', v', p', Y', Z']}} \times \underbrace{21,100}_{\#\,\mathrm{elements}} = 506,400$$

Computing the solution for a single frequency on this mesh on a Windows workstation, with 16GB of RAM and an Intel i7-4790 CPU @ 3.60 GHz, takes roughly 2 minutes.

Boundary Conditions

Boundary conditions (BC) are set as follows:

- Inlet: Dirichlet BC for all variables, except for $\nabla p'$ (von Neumann BC)
- Outlet: von Neumann BC for all variables, except for p' (Dirichlet BC).
- Slit wall:
  - Attached flame:(adiabatic, no-slip wall) Dirichlet BC for temperature, velocities equal zero (Dirichlet BC), von Neumann BC for pressure and mass fractions.
  - Lifted flame: (fixed temperature, no-slip wall) Dirichlet BC for temperature, velocities equal zero (Dirichlet BC), von Neumann BC for pressure and mass fractions.

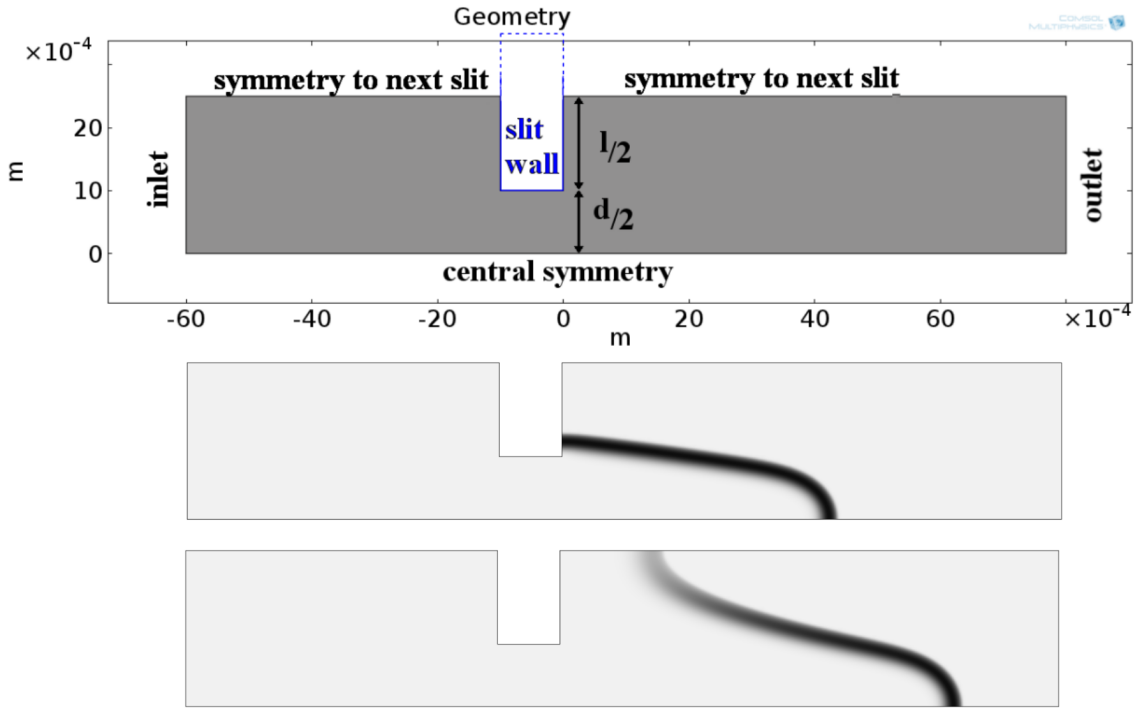

Figure 5.2: Computational domain in COMSOL (top), mean heat release rate of the attached flame (middle) and the lifted flame (bottom).

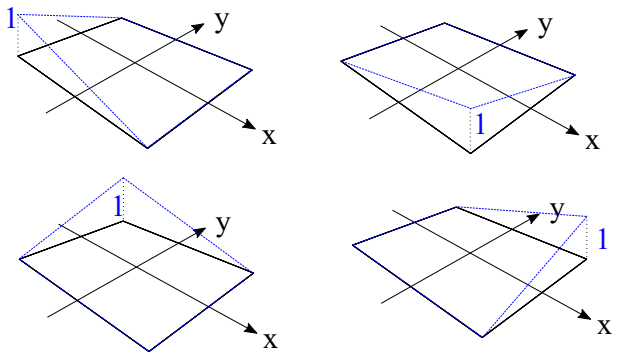

Figure 5.3: Linear test functions (normalized,blue) on a 2D quadratic element

- Symmetries (central and to next slit): von Neumann BC for all variables, except for v' (Dirichlet BC).

Note that, temperature BCs are fulfilled by the corresponding relations between ρ', p' and Z' from the LIGL (see eqns. (2.10) and (3.18)). Explicit mathematical formulations for these BC are given in tab. 5.1.

For the CFD calculations of reference FRF and mean fields the following BC are set: isothermal fixed-velocity fixed-mixture inlet where velocity is 0.30 m/s at an inlet temperature of 293 K. The inlet equivalence ratio is 0.8, giving mass fractions $Y_{CH_4,0} = 0.0445$, $Y_{O_2,0} = 0.2227$

	Inlet	Adiabatic wall	Fixed temperature wall	Symmetry	Outlet
Density ρ'	$\frac{p'}{\overline{p}} - \frac{\rho'}{\overline{\rho}} - k_{\sum Y'} Z' = 0$	$\vec{n} \cdot \nabla \rho' = 0$	$\frac{p'}{\overline{p}} - \frac{\rho'}{\overline{\rho}} - k_{\sum Y'} Z' = 0$	$\vec{n} \cdot \nabla \rho' = 0$	$\vec{n} \cdot \nabla \rho' = 0$
Velocity u'	$u' = u_{\text{exc}}$	$u' = 0$	$u' = 0$	$\vec{n} \cdot \nabla u' = 0$	$\vec{n} \cdot \nabla u' = 0$
Velocity v'	$v' = 0$	$v' = 0$	$v' = 0$	$v' = 0$	$\vec{n} \cdot \nabla v' = 0$
Pressure p'	$\vec{n} \cdot \nabla p' = 0$	$\vec{n} \cdot \nabla p' = 0$	$\vec{n} \cdot \nabla p' = 0$	$\vec{n} \cdot \nabla p' = 0$	$p' = 0$
Mass frac. Y'	$Y' = Y_{\text{exc}}$	$\vec{n} \cdot \nabla Y' = 0$	$\vec{n} \cdot \nabla Y' = 0$	$\vec{n} \cdot \nabla Y' = 0$	$\vec{n} \cdot \nabla Y' = 0$
Mass frac. Z'	$(1 + \gamma_{air}) Z' + Y_{\text{exc}} = 0$	$\vec{n} \cdot \nabla Z' = 0$	$\vec{n} \cdot \nabla Z' = 0$	$\vec{n} \cdot \nabla Z' = 0$	$\vec{n} \cdot \nabla Z' = 0$

Table 5.1: Boundary conditions setting

and $Y_{N_2,0} = 0.7328$. Outlet pressure is fixed at 101325 Pa. The non-slip slit wall has a constant temperature of 375 K for the lifted flame, whereas it is handled with zero heat flux for the attached flame.

Reference data

The reference FRFs for velocity and equivalence ratio perturbations are obtained in OpenFOAM with a broadband excitation of 5 % amplitude at the inlet to ensure the linear flame response. The LES is run for 0.13 s with CFL = 0.1. The FRF is identified as a finite impulse response (FIR) with 95 % accuracy. For robustness, a weakly compressible solver in OpenFOAM is used, with fixed pressure in the ideal gas law. Thus, density is only dependent on temperature and any thermoacoustic instabilities are suppressed. This OpenFOAM setup was earlier applied in [14] for velocity excitations and is adopted for equivalence ratio perturbations in a similar manner. The reference flame responses were provided by supervisor Alexander Avdonin. For detailed information on the identification procedure the reader should consult Tay-Wo-Chong et al. [12] and Polifke [13].

Study of velocity perturbations

The application of the LRF solver to velocity perturbations was recently done by Avdonin et al. [14]. It is run with velocity inlet excitation $u_{\text{exc}} = 1$ over a frequency band from 0 Hz to 500 Hz. Results are presented in fig. 5.4.

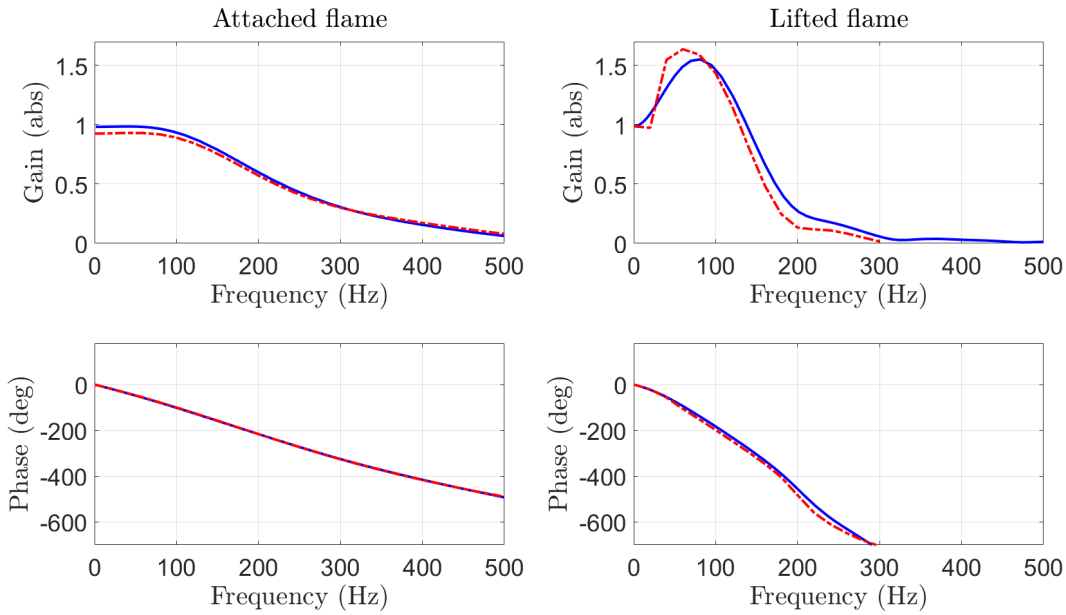

Figure 5.4: Frequency response for velocity perturbations for the attached (left) and lifted flame (right) identified from CFD simulations (—) and computed by the LRF solver (· –).

The LRF model accurately predicts the phase of the frequency response, showing that transport of the flow variables is reproduced correctly. This is an important feature, as the linearization of the heat release with an Arrhenius ansatz (eq. (2.21)) relies upon the precise transport of reacting species to and through the flame.

The gain of the attached flame is captured well, too. The lifted flame exhibts excess gain in the regions around 80 Hz, with an overestimate of up to 15 % for the DG-LRF solutions. The characteristics of the reference FTF are also found in the LRF-FTF: In the range from 0 to 80 Hz, the gain rises to a maximum, and then drops to almost zero starting with frequencies higher than 300 Hz.

5.2 Study of equivalence ratio perturbations

For the study of equivalence ratio perturbations a modulation of methane's mass fraction Y' is prescribed at the inlet, while u_{exc} is set to zero. Note, that for the computation of flame response functions F_ϕ, at least one more species equation has to be solved in the coupled system than for velocity perturbations. Additionally, the decoupled transport of Z is simulated. Thus, the study of eqivalence ration perturbations in slightly more expensive.

Figure 5.5 shows the flame responses F_ϕ obtained from the LRF with the YZ reduction and with all species equations solved ('LRF - Full'). The LRF solutions were computed on meshes with grid spacing of 40μm and 25μm. They are compared to the FRF from CFD identification, that was computed on a uniform mesh of element size Δx = 25μm with an accuracy of more than 95%. Therefore, confidence intervals are small and not shown in plots.

Both flames exhibit low-pass filter characteristics, where the phase slope is almost constant for frequencies with considerable gain. For each flame a frequency band with excessive gain is apparent, which has its peak around 30 Hz for the attached flame. The lifted flame shows stronger excessive gain around frequencies of 25 Hz. The gain then decays for both flames, until the response approaches zero for excitation higher than 200 Hz.

As for velocity excitation, the phase is precisely predicted by all LRF solutions. This shows that transport of species is reproduced correctly.

The gain in frequency response is fairly well captured by the LRF-YZ solver for the lifted flame, but the peak gain is displayed at 30 Hz. For the attached flame, however, the solution shows no excessive gain for the frequency band from 0 to 50 Hz, underestimating the reference data up to 20%.

The LRF-Full solver solution for the attached flame is not distinguishable from the one computed with the reduced LRF-YZ model. Thus, it can be deduced that the reduced model performs equally well and saves computational effort.

In summary, the LRF solution for equivalence ratio perturbations shows good capture of transport dynamics as the phase of FRFs agrees with the reference data. The gain is predicted with noticeable underestimation in the excessive frequency band for the attached flame, and with just a slight overestimate and peak displacement for the lifted flame. Overall the gain trends are captured sufficiently by the LRF solutions.

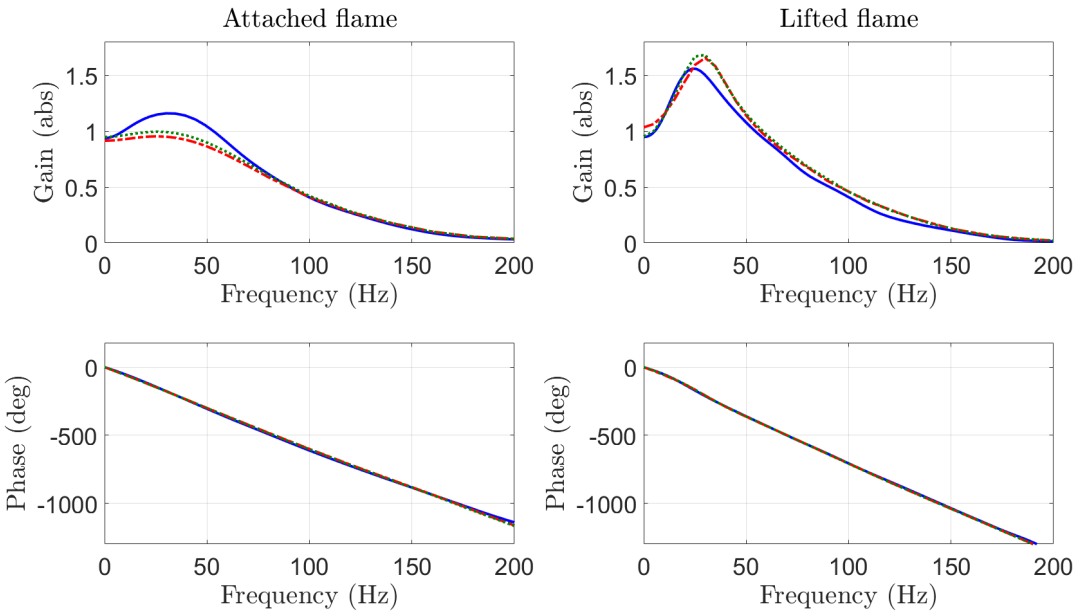

Figure 5.5: Frequency response for equivalence ratio perturbations for the attached (left) and lifted flame (right) identified from CFD simulations (—) and computed by the LRF solver with reduced YZ-equations on mesh with $\Delta x = 40\mu m$ ($\cdot -$) and with $\Delta x = 25\mu m$ ($\cdots$).

5.3 Study of parametric influences

For the study of the influence of the mass fractions' term in the linearized gas law $k_{\sum Y'}Z$ and of the enthalpy perturbations due to mass fraction perturbations $\sum_k \overline{h}_{Y_k} Y_k'$, only the LRF-YZ equations are applied. This study investigates, if further modelling simplifications can be made with reasonable accuracy.

Figure 5.6 shows the results of this examination. Omitting any of the two effects in simulation has no influence on the phase prediction. The negligence of mass fractions in the ideal gas law ($k_{\sum Y'}Z = 0$) also is not noticeable in the gain values. If enthalpy perturbations from mass faction fluctuations are switched off ($\sum_k \overline{h}_{Y_k} Y_k' = 0$), the gain for each flame increases up to around 10% for both flame configurations.

We can conclude, that temperature perturbations are only weakly linked to mass fraction perturbations by the linearized ideal gas law. This term could be omitted. Perturbations of species mixture, however, have an effect on enthalpy perturbations and influence results notably. They should therefore be taken into account.

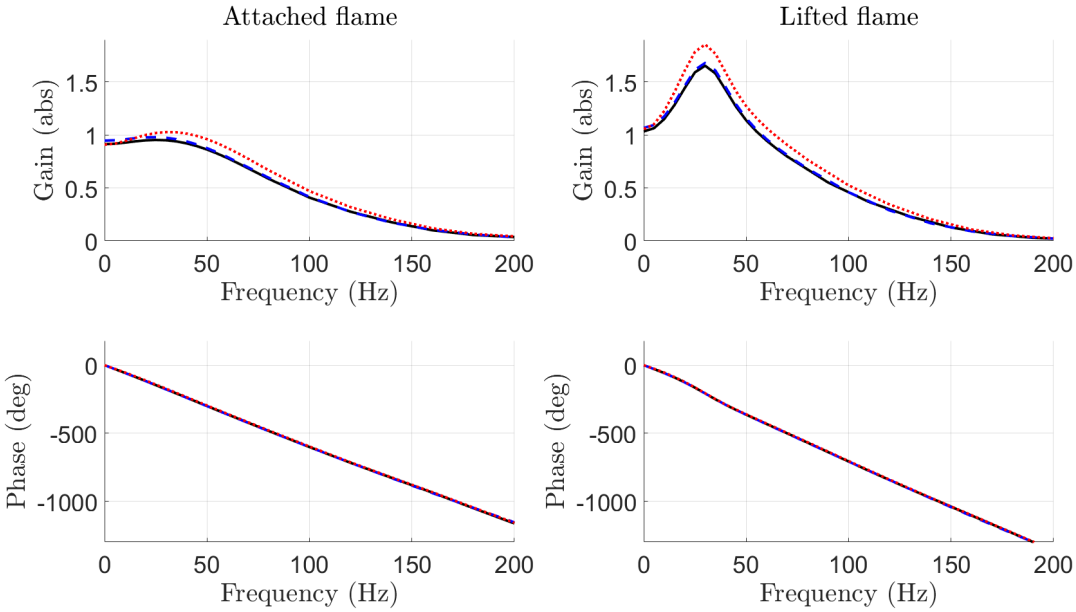

Figure 5.6: Frequency response for equivalence ratio perturbations computed by the LRF solver (—) compared to $k_{\sum Y'} = 0$ (- -) and $\overline{h}_Y = 0$ (···).

6 Conclusion and Outlook

Main focus of the thesis is the application of LRF to equivalence ratio perturbations. LRF poses a simulation method, that demands less time and computation power than LES. The approach relies on solving LNSE discretized by DG-FEM in frequency domain.

The first part shows the deduction of linearized reacting flow equations including linearized reaction rates modeled with Arrhenius' law. An approach to reduce the number of independent variables is explained, that expresses the five involved species by only two variables using stoichiometric relations. By solving for less DOFS, the requirements on storage and processing power are minimized further. The PDEs are discretized with the discontinuous Galerkin FEM and solved in frequency domain.

Then, the reduced and full models are applied to compute the flame response functions of laminar, premixed flames in 2D. Two boundary conditions are examined yielding either an attached or a lifted flame.

For the case of equivalence ratio perturbations, the phase from all LRF solutions is in good agreement with the CFD solutions, suggesting that the transport of flow variable perturbations including species transport is reproduced well. The gain computed on the LRF equations, however, differs from the reference FRF: for the attached flame the excess gain frequency band is not resolved, whereas the gain peak is predicted at a somewhat higher frequency for the lifted flame.

The study of the influence of including mass fraction perturbations into the linearization of the ideal gas law and sensible enthalpy is presented as well. It shows, that mass fraction perturbations can be neglected for the ideal gas law, while their influence in enthalpy perturbations has to be considered.

Due to satisfactory results in gain prediction and accurate phase representation for equivalence ratio perturbations, FRF determination based on LRF shows promising aspects and is computationally far less expensive than identification from CFD time series. With more sophisticated meshing, that better resolves the flame region and therefore reduces modeling errors in the reactive terms, more accurate results should be obtained.

Furthermore, LRF solvers could be applied for analysis of thermoacoustic modes, that require the solution of eigenvalue problems. This was already done for velocity perturbations in [14].

Also, the extension to turbulent flames is desirable, though here much finer spatial resolution is necessary, and the number of DOFs is increased. Furthermore, turbulence modeling and capturing interference between turbulence and chemical reactions have to be dealt with.

Appendices

A Detailed Linearization

This appendix shows detailed deductions for the LNSE as described in chapter 2.2.

A.1 Momentum conservation

Including explicit formulations for the vicious stress tensor, the momentum conservation equations read in index notation:

$$\underbrace{\frac{\partial \rho u_i}{\partial t}}_{①} + \underbrace{\frac{\partial \rho u_i u_j}{\partial x_j}}_{②} = \underbrace{-\frac{\partial p}{\partial x_i}}_{③} + \underbrace{\frac{\partial}{\partial x_j}\mu\left(\frac{\partial u_i}{\partial x_j} + \frac{\partial u_j}{\partial x_i} - \frac{2}{3}\delta_{ij}\frac{\partial u_k}{\partial x_k}\right)}_{④} \tag{A.1}$$

The terms ① to ④ are now formulated individually:

$$① = \frac{\partial(\overline{\rho}+\rho')(\overline{u_i}+u_i')}{\partial t} = \left[\frac{\partial \overline{\rho u_i}}{\partial t}\right] + \frac{\partial \rho' \overline{u_i}}{\partial t} + \frac{\partial \overline{\rho} u_i'}{\partial t} + \underbrace{\frac{\partial \rho' u_i'}{\partial t}}_{\text{HO term}}$$

$$\begin{aligned} ② &= \frac{\partial(\overline{\rho}+\rho')(\overline{u_i}+u_i')(\overline{u_j}+u_j')}{\partial x_j} \\ &= \left[\frac{\partial \overline{\rho u_i u_j}}{\partial x_j}\right] + \frac{\partial \overline{\rho u_i} u_j'}{\partial x_j} + \frac{\partial \overline{\rho} u_i' \overline{u_j}}{\partial x_j} + \frac{\partial \rho' \overline{u_i u_j}}{\partial x_j} + \underbrace{\frac{\partial \overline{\rho} u_i' u_j'}{\partial x_j} + \frac{\partial \rho' \overline{u_i} u_j'}{\partial x_j} + \frac{\partial \rho' u_i' \overline{u_j}}{\partial x_j} + \frac{\partial \rho' u_i' u_j'}{\partial x_j}}_{\text{HO terms}} \end{aligned}$$

$$③ = \left[-\frac{\partial \overline{p}}{\partial x_i} \right] - \frac{\partial p'}{\partial x_i}$$

$$\begin{aligned} ④ &= \frac{\partial}{\partial x_j}(\overline{\mu}+\mu')\left(\frac{\partial}{\partial x_j}(\overline{u_i}+u_i') + \frac{\partial}{\partial x_i}(\overline{u_j}+u_j') - \frac{2}{3}\delta_{ij}\frac{\partial}{\partial x_k}(\overline{u_k}+u_k')\right) \\ &= \left[\frac{\partial}{\partial x_j}\overline{\mu}\left(\frac{\partial \overline{u}_i}{\partial x_j} + \frac{\partial \overline{u}_j}{\partial x_i} - \frac{2}{3}\delta_{ij}\frac{\partial \overline{u}_k}{\partial x_k}\right)\right] + \frac{\partial}{\partial x_j}\mu'\left(\frac{\partial \overline{u}_i}{\partial x_j} + \frac{\partial \overline{u}_j}{\partial x_i} - \frac{2}{3}\delta_{ij}\frac{\partial \overline{u}_k}{\partial x_k}\right) \\ &\quad + \frac{\partial}{\partial x_j}\overline{\mu}\left(\frac{\partial u_i'}{\partial x_j} + \frac{\partial u_j'}{\partial x_i} - \frac{2}{3}\delta_{ij}\frac{\partial u_k'}{\partial x_k}\right) + \underbrace{\frac{\partial}{\partial x_j}\mu'\left(\frac{\partial u_i'}{\partial x_j} + \frac{\partial u_j'}{\partial x_i} - \frac{2}{3}\delta_{ij}\frac{\partial u_k'}{\partial x_k}\right)}_{\text{HO term}} \end{aligned}$$

Applying the MVP, the terms in square brackets are left out from the equation, as well as HO terms.

The complete linearized momentum equation reads:

$$\begin{aligned} &\frac{\partial \rho' \overline{u_i}}{\partial t} + \frac{\partial \overline{\rho} u_i'}{\partial t} + \frac{\partial \overline{\rho u_i} u_j'}{\partial x_j} + \frac{\partial \overline{\rho} u_i' \overline{u_j}}{\partial x_j} + \frac{\partial \rho' \overline{u_i u_j}}{\partial x_j} = \\ &\quad -\frac{\partial p'}{\partial x_i} + \frac{\partial}{\partial x_j}\mu'\left(\frac{\partial \overline{u}_i}{\partial x_j} + \frac{\partial \overline{u}_j}{\partial x_i} - \frac{2}{3}\delta_{ij}\frac{\partial \overline{u}_k}{\partial x_k}\right) + \frac{\partial}{\partial x_j}\overline{\mu}\left(\frac{\partial u_i'}{\partial x_j} + \frac{\partial u_j'}{\partial x_i} - \frac{2}{3}\delta_{ij}\frac{\partial u_k'}{\partial x_k}\right) \end{aligned} \tag{A.2}$$

The formulae for x- and y-momentum are given in section 2.3, with the viscous terms written out specificially.

A.2 Species conservation

The species equation for species k is being linearized in terms as follows:

$$\underbrace{\frac{\partial \rho Y_k}{\partial t}}_{①} + \underbrace{\frac{\partial \rho u Y_k}{\partial x}}_{②} + \underbrace{\frac{\partial \rho v Y_k}{\partial y}}_{③} = \underbrace{\frac{\partial}{\partial x}\left(D\frac{\partial Y_k}{\partial x}\right)}_{④} + \underbrace{\frac{\partial}{\partial y}\left(D\frac{\partial Y_k}{\partial y}\right)}_{⑤} + \underbrace{\dot{\omega}_i}_{⑥} \tag{A.3}$$

$$① = \frac{\partial(\overline{\rho}+\rho')(\overline{Y}_k + Y_k')}{\partial t} = \left[\frac{\partial \overline{\rho}\overline{Y}_k}{\partial t}\right] + \frac{\partial \rho' \overline{Y}_k}{\partial t} + \frac{\partial \overline{\rho} Y_k'}{\partial t} + \underbrace{\frac{\partial \rho' Y_k'}{\partial t}}_{\text{HO term}}$$

$$\begin{aligned} ② &= \frac{\partial(\overline{\rho}+\rho')(\overline{u}+u')(\overline{Y}_k + Y_k')}{\partial x} = \left[\frac{\partial \overline{\rho}\overline{u}\overline{Y}_k}{\partial x}\right] + \frac{\partial \overline{\rho}\overline{u} Y_k'}{\partial x} + \frac{\partial \overline{\rho} u' \overline{Y}_k}{\partial x} + \frac{\partial \rho' \overline{u}\overline{Y}_k}{\partial x} \\ &\quad + \underbrace{\frac{\partial \overline{\rho} u' Y_k'}{\partial x} + \frac{\partial \rho' \overline{u} Y_{CH_4'}}{\partial x} + \frac{\partial \rho' u' \overline{Y}_k}{\partial x} + \frac{\partial \rho' u' Y_k'}{\partial x}}_{\text{HO terms}} \end{aligned}$$

$$③ = \frac{\partial(\overline{\rho}+\rho')(\overline{v}+v')(\overline{Y}_k+Y_k')}{\partial y} = \left[\frac{\partial\overline{\rho}\,\overline{v}\,\overline{Y}_k}{\partial y}\right] + \frac{\partial\overline{\rho}\,\overline{v}\,Y_k'}{\partial y} + \frac{\partial\overline{\rho}\,v'\overline{Y}_k}{\partial y} + \frac{\partial\rho'\overline{v}\,\overline{Y}_k}{\partial y} + \underbrace{\frac{\partial\overline{\rho}\,v'Y_k'}{\partial y} + \frac{\partial\rho'\overline{v}\,Y_k'}{\partial y} + \frac{\partial\rho'v'\overline{Y}_k}{\partial y} + \frac{\partial\rho'v'Y_k'}{\partial y}}_{\text{HO terms}}$$

$$④ = \frac{\partial}{\partial x}\left((\overline{D}+D')\frac{\partial(\overline{Y}_k+Y_k')}{\partial x}\right)$$
$$= \left[\frac{\partial}{\partial x}\left(\overline{D}\frac{\partial\overline{Y}_k}{\partial x}\right)\right] + \frac{\partial}{\partial x}\left(\overline{D}\frac{\partial Y_k'}{\partial x}\right) + \frac{\partial}{\partial x}\left(D'\frac{\partial\overline{Y}_k}{\partial x}\right) + \underbrace{\frac{\partial}{\partial x}\left(D'\frac{\partial Y_k'}{\partial x}\right)}_{\text{HO term}}$$

$$⑤ = \frac{\partial}{\partial y}\left((\overline{D}+D')\frac{\partial(\overline{Y}_k+Y_k')}{\partial y}\right)$$
$$= \left[\frac{\partial}{\partial y}\left(\overline{D}\frac{\partial\overline{Y}_k}{\partial y}\right)\right] + \frac{\partial}{\partial y}\left(\overline{D}\frac{\partial Y_k'}{\partial y}\right) + \frac{\partial}{\partial y}\left(D'\frac{\partial\overline{Y}_k}{\partial y}\right) + \underbrace{\frac{\partial}{\partial y}\left(D'\frac{\partial Y_k'}{\partial y}\right)}_{\text{HO term}}$$

$$⑥ = \left[\overline{\dot{\omega}}_i\right] + \dot{\omega}_i'$$

After neglecting higher order terms and applying the MVP (terms in square brackets), the linearized 2D species equation reads:

$$\frac{\partial\rho'\overline{Y}_k}{\partial t} + \frac{\partial\overline{\rho}\,Y_k'}{\partial t} + \frac{\partial\overline{\rho}\,\overline{u}\,Y_k'}{\partial x} + \frac{\partial\overline{\rho}\,u'\overline{Y}_k}{\partial x} + \frac{\partial\rho'\overline{u}\,\overline{Y}_k}{\partial x} + \frac{\partial\overline{\rho}\,\overline{v}\,Y_k'}{\partial y} + \frac{\partial\overline{\rho}\,v'\overline{Y}_k}{\partial y} + \frac{\partial\rho'\overline{v}\,\overline{Y}_k}{\partial y} = \frac{\partial}{\partial x}\left(\overline{D}\frac{\partial Y_k'}{\partial x}\right) + \frac{\partial}{\partial x}\left(D'\frac{\partial\overline{Y}_k}{\partial x}\right) + \frac{\partial}{\partial y}\left(\overline{D}\frac{\partial Y_k'}{\partial y}\right) + \frac{\partial}{\partial y}\left(D'\frac{\partial\overline{Y}_k}{\partial y}\right) + \dot{\omega}_i{}' \tag{A.4}$$

A.3 Sensible enthalpy conservation

In similar fashion, the enthalpy equation will be linearized in seperate terms and then recompiled. The non-linear form reads:

$$\underbrace{\frac{\partial}{\partial t}\left(\rho h - p\right)}_{①} + \underbrace{\frac{\partial}{\partial x}\left(\rho u h\right)}_{②} + \underbrace{\frac{\partial}{\partial y}\left(\rho v h\right)}_{③} = \underbrace{\dot{\omega}_T}_{④} + \underbrace{\frac{\partial}{\partial x}\alpha\frac{\partial h}{\partial x}}_{⑤} + \underbrace{\frac{\partial}{\partial y}\alpha\frac{\partial h}{\partial y}}_{⑥} \tag{A.5}$$

$$① = \frac{\partial}{\partial t}\Big((\overline{\rho}+\rho')(\overline{h}+h') - (\overline{p}+p')\Big) = \left[\frac{\partial}{\partial t}\Big(\overline{\rho h} - \overline{p}\Big)\right] + \frac{\partial}{\partial t}\Big(\rho'\overline{h} + \overline{\rho}h' - p'\Big) + \text{HO terms}$$

$$\begin{aligned} ② &= \frac{\partial}{\partial x}\Big((\overline{\rho}+\rho')(\overline{u}+u')(\overline{h}+h')\Big) \\ &= \left[\frac{\partial}{\partial x}\Big(\overline{\rho u h}\Big)\right] + \frac{\partial}{\partial x}\Big(\overline{\rho u}h' + \overline{\rho}u'\overline{h} + \rho'\overline{u}\overline{h}\Big) + \text{HO terms} \end{aligned}$$

$$\begin{aligned} ③ &= \frac{\partial}{\partial y}\Big((\overline{\rho}+\rho')(\overline{v}+v')(\overline{h}+h')\Big) \\ &= \left[\frac{\partial}{\partial y}\Big(\overline{\rho v h}\Big)\right] + \frac{\partial}{\partial y}\Big(\overline{\rho v}h' + \overline{\rho}v'\overline{h} + \rho'\overline{v}\overline{h}\Big) + \text{HO terms} \end{aligned}$$

$$④ = \overline{\dot{\omega}}_T + \dot{\omega}'_T$$

$$⑤ = \frac{\partial}{\partial x}\Big((\overline{\alpha}+\alpha')\frac{\partial(\overline{h}+h')}{\partial x}\Big) = \left[\frac{\partial}{\partial x}\overline{\alpha}\frac{\partial\overline{h}}{\partial x}\right] + \frac{\partial}{\partial x}\alpha'\frac{\partial\overline{h}}{\partial x} + \frac{\partial}{\partial x}\overline{\alpha}\frac{\partial h'}{\partial x} + \text{HO term}$$

$$⑥ = \frac{\partial}{\partial y}\Big((\overline{\alpha}+\alpha')\frac{\partial(\overline{h}+h')}{\partial y}\Big) = \left[\frac{\partial}{\partial y}\overline{\alpha}\frac{\partial\overline{h}}{\partial y}\right] + \frac{\partial}{\partial y}\alpha'\frac{\partial\overline{h}}{\partial y} + \frac{\partial}{\partial y}\overline{\alpha}\frac{\partial h'}{\partial y} + \text{HO term}$$

Once again, the MVP-terms in square brackets are subtracted and terms of quadratic order or higher omitted. Thus, the complete linearized Energy equation is obtained:

$$\begin{aligned} \frac{\partial}{\partial t}\Big(\rho'\overline{h} + \overline{\rho}h' - p'\Big) + \frac{\partial}{\partial x}\Big(\overline{\rho u}h' + \overline{\rho}u'\overline{h} + \rho'\overline{u}\overline{h}\Big) + \frac{\partial}{\partial y}\Big(\overline{\rho v}h' + \overline{\rho}v'\overline{h} + \rho'\overline{v}\overline{h}\Big) = \\ \dot{\omega}'_T + \frac{\partial}{\partial x}\alpha'\frac{\partial\overline{h}}{\partial x} + \frac{\partial}{\partial x}\overline{\alpha}\frac{\partial h'}{\partial x} + \frac{\partial}{\partial y}\alpha'\frac{\partial\overline{h}}{\partial y} + \frac{\partial}{\partial y}\overline{\alpha}\frac{\partial h'}{\partial y} \end{aligned} \tag{A.6}$$

B Analytical examination of reformulations in section 3.2

B.1 Analytical examination

This appendix gives a detailed analytical examination of eqns. (3.8) to (3.17). To show that the given formulae are correct, two relations must be fulfilled:

1. $\sum_i Y_i = \sum_i (\overline{Y}_i + Y'_i) \stackrel{!}{=} 1$ and
2. consequently: $\sum_i Y_i \stackrel{!}{=} 0$, since $\sum_i \overline{Y}_i = 1$ is fulfilled by the mean fields by definition of the MVP. The correctness of $\sum_i \overline{Y}_i = 1$ was further checked with a MATLAB script. The main parts and result of this script are explained in the second section.

Proof for constraint 1:

$$
\begin{aligned}
1 \stackrel{!}{=} \sum_i Y_i &= Y_{N2} + Y_{CH_4} + Y_{O_2} + Y_{CO_2} + Y_{H_2O} \\
&= Z + Y + \gamma_{\text{air}} Z - s\Big(1 - \big(1+\gamma_{\text{air}}\big)Z - Y\Big) + \frac{W_{CO_2} + 2\,W_{H_2O}}{W_{CH_4}}\Big(1 - \big(1+\gamma_{\text{air}}\big)Z - Y\Big) \\
&= \underbrace{\Big(1 + s - \frac{W_{CO_2} + 2\,W_{H_2O}}{W_{CH_4}}\Big)}_{= 1 + \frac{2\cdot 32}{16} - \frac{44+2\cdot 18}{16} = 0} \big(1+\gamma_{\text{air}}\big)\, Z + \underbrace{\Big(1 + s - \frac{W_{CO_2} + 2\,W_{H_2O}}{W_{CH_4}}\Big)}_{= 1 + \frac{2\cdot 32}{16} - \frac{44+2\cdot 18}{16} = 0} Y \\
&\quad - s + \frac{W_{CO_2} + 2\,W_{H_2O}}{W_{CH_4}} = -4 + 5 = 1 \qquad \text{q.e.d.}
\end{aligned}
\tag{B.1}
$$

Proof for constraint 2:

$$
\begin{aligned}
0 \stackrel{!}{=} \sum_i Y'_i &= Y'_{N2} + Y'_{CH_4} + Y'_{O_2} + Y'_{CO_2} + Y'_{H_2O} \\
&= Z' + Y' + \gamma_{\text{air}} Z' + s'\Big(\big(1+\gamma_{\text{air}}\big)Z' + Y'\Big) - \frac{W_{CO_2} + 2\,W_{H_2O}}{W_{CH_4}}\Big(\big(1+\gamma_{\text{air}}\big)Z' + Y'\Big) \\
&= \underbrace{\Big(1 + s - \frac{W_{CO_2} + 2\,W_{H_2O}}{W_{CH_4}}\Big)}_{= 1 + \frac{2\cdot 32}{16} - \frac{44+2\cdot 18}{16} = 0} \big(1+\gamma_{\text{air}}\big)\, Z + \underbrace{\Big(1 + s - \frac{W_{CO_2} + 2\,W_{H_2O}}{W_{CH_4}}\Big)}_{= 1 + \frac{2\cdot 32}{16} - \frac{44+2\cdot 18}{16} = 0} Y = 0 \qquad \text{q.e.d.}
\end{aligned}
\tag{B.2}
$$

B.2 MATLAB check-up

In order to check, if mass fraction formulations are correct, they are tested with the following MATLAB script. A dimensionless domain is defined by:

```
% Domain settings

    start_reac_zone =0.55;
    end_reac_zone   =0.65;
    delta_x_reac    =0.002;
    delta_x_no_reac =0.05;

    x_l     =0:delta_x_no_reac:start_reac_zone;
    x_reac  =start_reac_zone:delta_x_reac:end_reac_zone;
    x_r     =end_reac_zone:delta_x_no_reac:1;

    x   =[x_l x_reac x_r]';
```

The combustion progress is described with a cumulative distribution function for progress variable ξ:

```
% Progress variable xi (defined by CDF)

    mu      = 0;
    sigma   = sqrt(0.06);
    pd      = makedist('Normal',0,sqrt(0.06));
    reac_zone=linspace(-1,1,length(x_reac));
    xi_reac =cdf(pd,reac_zone);
    xi_l    =zeros(size(x_l));
    xi_r    =ones(size(x_r));

    xi      =[xi_l xi_reac xi_r]';
```

Combustion progress

The progress variable ξ describes the combustion's development. For $\xi = 0$, methane is completely unburnt and the mixture consists of only methane and air. For $\xi = 1$, all the CH_4 is burnt and the mixture contains fractions of carbon dioxide, vaporized water, nitrogen and oxygen that was not consummated by the reaction.

$$\xi = \frac{Y_{CH_4,0} - Y_{CH_4}}{Y_{CH_4,0}}$$

With this definition, ξ takes values between 0 and 1, and will always develop as is shown in fig. 3.1 for lean combustion. There, the case of stoichiometric combustion in 1D is shown

with typical developments of fuel and oxidizer mass fractions, temperature, reaction rate and progress variable.

For the model from section 3.2, mass fractions are calculated by:

```
Z(:,k)       =Y_N2_0(k).*ones(size(x));
Y_CH4(:,k)   =(ones(size(x)) - x).*Y_CH4_0(k);
Y_O2(:,k)    =air_mix*Z(:,k)-s*(ones(size(x))...
                              -(1+air_mix)*Z(:,k)-Y_CH4(:,k));
Y_H2O(:,k)   =(2*W_H2O/W_CH4)*(ones(size(x))...
                              -(1+air_mix)*Z(:,k)-Y_CH4(:,k));
Y_CO2(:,k)   =(W_CO2/W_CH4)*(ones(size(x))...
                              -(1+air_mix)*Z(:,k)-Y_CH4(:,k));
```

Here, the progress variable ξ is imposed on the methane mass fraction Y_{CH_4} in order to 'simulate' combustion. Whether mass fractions add up to one, is checked for every point in the domain:

```
Y_tot(:,k) = Y_CH4(:,k) + Y_O2(:,k) ...
            + Y_CO2(:,k) + Y_H2O(:,k) + Z(:,k);

    % Y_checker
    Y_checker=Y_tot(:,k);
    for n=1:length(Y_checker)
        if abs((1-Y_checker(n)))>1e-4
            error ('Mass fractions dont add up!')
        end
    end
```

The result is shown in fig. B.1 and indicates that eqns. (3.8) to (3.12) correctly represent the mass fractions, since the constraint $\sum_i Y_i \stackrel{!}{=} 1$ is fulfilled at all points and for different equivalence ratios.

The calculations represent a premixed, laminar flame in 1D as presented in fig. 3.1. The flame region for this program is situated around $x/l = 0.6$. The development of each species is shown for example equivalence ratios of $\phi = 0.95$, 0.8 and 0.6. The sum of mass fractions is exactly 1 in all cases. Furthermore the plot in the bottom-right shows, that this is also true for every other equivalence ratio.

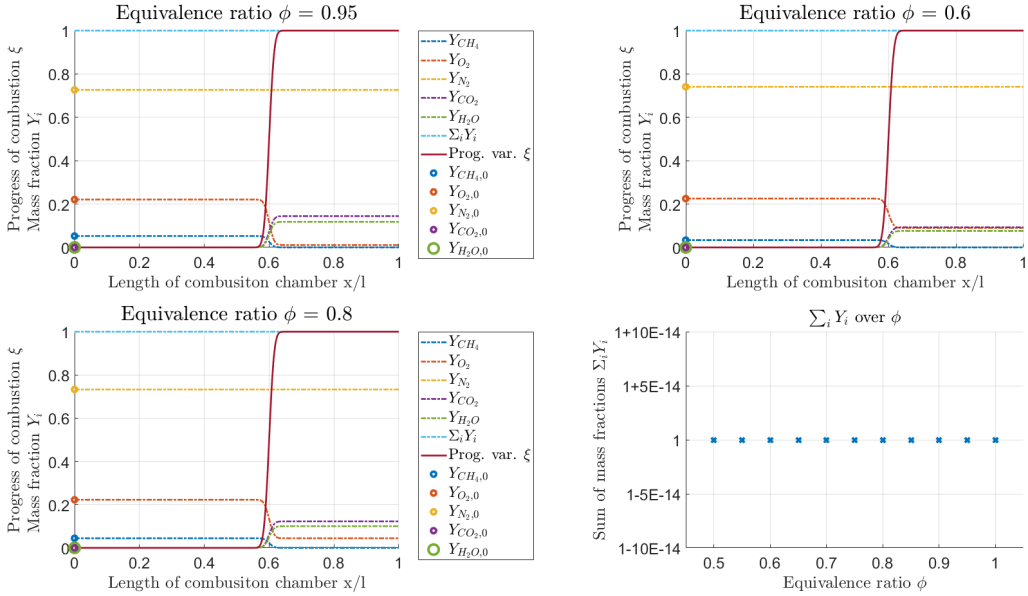

Figure B.1: Mass fractions Y_i, initial values $Y_{i,0}$ and combustion progress ξ in development over the domain as computed in MATLAB for values of ϕ from 0.5 to 1.

C Discontinous Galerkin form of the LNSE

This appendix lists the full formulations for the remaining DG-form of the LRF as they are introduced in chapter 4, and shortened to table 4.1.

C.1 x-Momentum equation

$$\begin{aligned}
&\int_{\Omega_e} l_u \frac{\partial}{\partial t}\left[\rho'\overline{u}+\overline{\rho}u'\right] - \left[\frac{\partial l_u}{\partial x}\left(\rho'\overline{u}^2+2\overline{\rho u}u'+p'-\overline{\mu}(\frac{4}{3}\frac{\partial u'}{\partial x}-\frac{2}{3}\frac{\partial v'}{\partial y})-\mu'(\frac{4}{3}\frac{\partial \overline{u}}{\partial x}-\frac{2}{3}\frac{\partial \overline{v}}{\partial y})\right)\right.\\
&\quad\left.+\frac{\partial l_u}{\partial y}\left(\rho'\overline{uv}+\overline{\rho}u'\overline{v}+\overline{\rho u}v'-\overline{\mu}(\frac{\partial u'}{\partial y}+\frac{\partial v'}{\partial x})-\mu'(\frac{\partial \overline{u}}{\partial y}+\frac{\partial \overline{v}}{\partial x})\right)\right] \quad d\Omega_e\\
&+\int_{\Gamma_e} \underbrace{l_u\left(\rho'\overline{u}^2+2\overline{\rho u}u'+p'-\overline{\mu}(\frac{4}{3}\frac{\partial u'}{\partial x}-\frac{2}{3}\frac{\partial v'}{\partial y})-\mu'(\frac{4}{3}\frac{\partial \overline{u}}{\partial x}-\frac{2}{3}\frac{\partial \overline{v}}{\partial y})\right)n_x}_{\substack{\text{normal flux in x-direction}\\ f_{\rho u,n_x}}}\\
&\quad+\underbrace{l_u\left(\rho'\overline{uv}+\overline{\rho}u'\overline{v}+\overline{\rho u}v'-\overline{\mu}(\frac{\partial u'}{\partial y}+\frac{\partial v'}{\partial x})-\mu'(\frac{\partial \overline{u}}{\partial y}+\frac{\partial \overline{v}}{\partial x})\right)n_y}_{\substack{\text{normal flux in y-direction}\\ f_{\rho u,n_y}}} \quad d\Gamma_e = 0
\end{aligned} \tag{C.1}$$

C.2 y-Momentum equation

$$\begin{aligned}
&\int_{\Omega_e} l_v \frac{\partial}{\partial t}\left[\rho'\overline{v}+\overline{\rho}v'\right] - \left[\frac{\partial l_v}{\partial y}\left(\rho'\overline{v}^2+2\overline{\rho v}v'+p'-\overline{\mu}(\frac{4}{3}\frac{\partial v'}{\partial y}-\frac{2}{3}\frac{\partial u'}{\partial x})-\mu'(\frac{4}{3}\frac{\partial \overline{v}}{\partial y}-\frac{2}{3}\frac{\partial \overline{u}}{\partial x})\right)\right.\\
&\quad\left.+\frac{\partial l_v}{\partial x}\left(\rho'\overline{uv}+\overline{\rho}u'\overline{v}+\overline{\rho u}v'-\overline{\mu}(\frac{\partial u'}{\partial y}+\frac{\partial v'}{\partial x})-\mu'(\frac{\partial \overline{u}}{\partial y}+\frac{\partial \overline{v}}{\partial x})\right)\right] \quad d\Omega_e\\
&+\int_{\Gamma_e} \underbrace{l_v\left(\rho'\overline{v}^2+2\overline{\rho v}v'+p'-\overline{\mu}(\frac{4}{3}\frac{\partial v'}{\partial y}-\frac{2}{3}\frac{\partial u'}{\partial x})-\mu'(\frac{4}{3}\frac{\partial \overline{v}}{\partial y}-\frac{2}{3}\frac{\partial \overline{u}}{\partial x})\right)n_y}_{\substack{\text{normal flux in y-direction}\\ f_{\rho v,n_y}}}\\
&\quad+\underbrace{l_v\left(\rho'\overline{uv}+\overline{\rho}u'\overline{v}+\overline{\rho u}v'-\overline{\mu}(\frac{\partial u'}{\partial y}+\frac{\partial v'}{\partial x})-\mu'(\frac{\partial \overline{u}}{\partial y}+\frac{\partial \overline{v}}{\partial x})\right)n_x}_{\substack{\text{normal flux in x-direction}\\ f_{\rho v,n_x}}} \quad d\Gamma_e = 0
\end{aligned} \tag{C.2}$$

C.3 Species equation

$$
\begin{aligned}
&\int_{\Omega_e} l_{Y_i}\frac{\partial}{\partial t}\left[\rho'\overline{Y_i}+\overline{\rho}Y_i'\right]-l_{Y_i}\,\dot{\omega}_i'-\left[\frac{\partial l_{Y_i}}{\partial x}\left(\rho'\overline{u}\overline{Y_i}+\overline{\rho}u'\overline{Y_i}+\overline{\rho u}Y_i'-\rho' D_i\frac{\partial\overline{Y}_i}{\partial x}-\overline{\rho}D_i\frac{\partial Y_i'}{\partial x}\right)\right.\\
&\qquad\left.+\frac{\partial l_{Y_i}}{\partial y}\left(\rho'\overline{v}\overline{Y_i}+\overline{\rho}v'\overline{Y_i}+\overline{\rho v}Y_i'-\rho' D_i\frac{\partial\overline{Y}_i}{\partial y}-\overline{\rho}D_i\frac{\partial Y_i'}{\partial y}\right)\right]d\Omega_e\\
&+\int_{\Gamma_e} l_{Y_i}\underbrace{\left(\rho'\overline{u}\overline{Y_i}+\overline{\rho}u'\overline{Y_i}+\overline{\rho u}Y_i'-\rho' D_i\frac{\partial\overline{Y}_i}{\partial x}-\overline{\rho}D_i\frac{\partial Y_i'}{\partial x})\right)n_x}_{\substack{\text{normal flux in x-direction}\\ f_{\rho Y_i,n_x}}}\\
&\qquad+l_{Y_i}\underbrace{\left(\rho'\overline{v}\overline{Y_i}+\overline{\rho}v'\overline{Y_i}+\overline{\rho v}Y_i'-\rho' D_i\frac{\partial\overline{Y}_i}{\partial y}-\overline{\rho}D_i\frac{\partial Y_i'}{\partial y}\right)n_y}_{\substack{\text{normal flux in y-direction}\\ f_{\rho Y_i,n_y}}}d\Gamma_e=0
\end{aligned}
\tag{C.3}
$$

C.4 Sensible Enthalpy equation

$$
\begin{aligned}
&\int_{\Omega_e} l_p\frac{\partial}{\partial t}\left[\rho'\overline{h}+\overline{\rho}h'-p'\right]-l_p\,\dot{\omega}_T'\\
&\qquad-\left[\frac{\partial l_p}{\partial x}\left(\rho'\overline{u}\overline{h}+\overline{\rho}u'\overline{h}+\overline{\rho u}h'\right)+\frac{\partial l_p}{\partial y}\left(\rho'\overline{v}\overline{h}+\overline{\rho}v'\overline{h}+\overline{\rho v}h'\right)\right]\\
&\qquad+\left[\frac{\partial l_p}{\partial x}\left(\overline{\alpha}\frac{\partial h'}{\partial x}+\alpha'\frac{\partial\overline{h}}{\partial x}\right)+\frac{\partial l_p}{\partial y}\left(\overline{\alpha}\frac{\partial h'}{\partial y}+\alpha'\frac{\partial\overline{h}}{\partial y}\right)\right]\quad d\Omega_e\\
&+\int_{\Gamma_e} l_p\underbrace{\left(\rho'\overline{u}\overline{h}+\overline{\rho}u'\overline{h}+\overline{\rho u}h'-\overline{\alpha}\frac{\partial h'}{\partial x}-\alpha'\frac{\partial\overline{h}}{\partial x}\right)n_x}_{\substack{\text{normal flux in x-direction}\\ f_{\rho h,n_x}}}\\
&\qquad+l_p\underbrace{\left(\rho'\overline{v}\overline{h}+\overline{\rho}v'\overline{h}+\overline{\rho v}h'-\overline{\alpha}\frac{\partial h'}{\partial y}-\alpha'\frac{\partial\overline{h}}{\partial y}\right)n_y}_{\substack{\text{normal flux in y-direction}\\ f_{\rho h,n_y}}}=0
\end{aligned}
\tag{C.4}
$$

D Correction factor for flame response function F_ϕ

This appendix shows the deduction of the correction factor for the conversion from mass fraction to equivalence ratio perturbations.

From the definition of the equivalence ratio in eq. (3.7) it can be rewritten to:

$$\phi = s\,\frac{Y_{CH_4}}{Y_{O_2}} = s\,\frac{(1+\gamma_{\text{air}})\,Y}{\gamma_{\text{air}}(1-Y)} \tag{D.1}$$

using

$$\begin{aligned} 1 &= Y_{CH_4} + Y_{O_2} + Y_{N_2} \\ 1 - Y &= Y_{O_2} + \frac{1}{\gamma_{\text{air}}} Y_{O_2} \\ Y_{O_2} &= \frac{\gamma_{\text{air}}(1-Y)}{1+\gamma_{\text{air}}}. \end{aligned}$$

From eq. (D.1) the linearization is obtained as:

$$\begin{aligned} \phi' = s\frac{1+\gamma_{\text{air}}}{\gamma_{\text{air}}}\frac{(1-\overline{Y})+\overline{Y}}{(1-\overline{Y})^2}\,Y' &= \overline{\phi}\frac{1}{1-\overline{Y}}\frac{Y'}{\overline{Y}} \\ \frac{\phi'}{\overline{\phi}} &= \frac{1}{1-\overline{Y}}\frac{Y'}{\overline{Y}} \end{aligned} \tag{D.2}$$

Thus, the correction factor for the flame response to equivalence ratio perturbations (cf. eq. (1.2)) calculation reads:

$$F_\phi = \frac{\dot{Q}'/\overline{\dot{Q}}}{\phi'/\overline{\phi}} = \frac{\dot{Q}'/\overline{\dot{Q}}}{Y'/\overline{Y}}\quad\underbrace{(1-\overline{Y})}_{\begin{array}{l}=1-0.0445\\=0.9555\end{array}} \tag{D.3}$$

Bibliography

[1] Denis Veynante and Luc Vervisch. Turbulent combustion modeling. *Progress in energy and combustion science*, 28(3):193–266, 2002.

[2] V. N. Kornilov, R. Rook, J. H M ten Thije Boonkkamp, and L. P H de Goey. Experimental and numerical investigation of the acoustic response of multi-slit Bunsen burners. *Combustion and Flame*, 156(10):1957–1970, 2009. ISSN 00102180. doi: 10.1016/j.combustflame.2009.07.017.

[3] Thierry Poinsot and Denis Veynante. *Theoretical and numerical combustion*. RT Edwards, Inc., 2005.

[4] A Albayrak, RS Blumenthal, A Ulhaq, and W Polifke. An analytical model for the impulse response of laminar premixed flames to equivalence ratio perturbations. *Proceedings of the Combustion Institute*, 36(3):3725–3732, 2017.

[5] AP Dowling and S Hubbard. Instability in lean premixed combustors. *Proceedings of the Institution of Mechanical Engineers, Part A: Journal of Power and Energy*, 214(4):317–332, 2000.

[6] Ju Hyeong Cho and Tim Lieuwen. Laminar premixed flame response to equivalence ratio oscillations. *Combustion and flame*, 140(1):116–129, 2005.

[7] Shreekrishna, Santosh Hemchandra, and Tim Lieuwen. Premixed flame response to equivalence ratio perturbations. *Combustion Theory and Modelling*, 14(5):681–714, 2010.

[8] Santosh Hemchandra. Direct numerical simulation study of premixed flame response to fuel-air ratio oscillations. In *Proceedings of ASME Turbo Expo*, 2011.

[9] T Emmert, S Bomberg, S Jaensch, and W Polifke. Acoustic and intrinsic thermoacoustic modes of a premixed combustor. *Proceedings of the Combustion Institute*, 36(3):3835–3842, 2017.

[10] Camilo F Silva, Malte Merk, Thomas Komarek, and Wolfgang Polifke. The contribution of intrinsic thermoacoustic feedback to combustion noise and resonances of a confined turbulent premixed flame. *Combustion and Flame*, 182:269–278, 2017.

[11] Camilo F. Silva, Thomas Emmert, Stefan Jaensch, and Wolfgang Polifke. Numerical study on intrinsic thermoacoustic instability of a laminar premixed flame. *Combustion and Flame*, 162(9):3370 – 3378, 2015. ISSN 0010-2180.

[12] Luis Tay-Wo-Chong, Sebastian Bomberg, Ahtsham Ulhaq, Thomas Komarek, and Wolfgang Polifke. Comparative validation study on identification of premixed flame transfer function. *Journal of Engineering for Gas Turbines and Power*, 134(2):021502, 2012.

[13] Wolfgang Polifke. Black-box system identification for reduced order model construction. *Annals of Nuclear Energy*, 67:109–128, 2014.

[14] A. Avdonin, M. Meindl, and W. Polifke. Thermoacoustic analysis of a laminar premixed flame using a linearized reactive flow solver. *Conference paper submitted to 37th Int'l Symposium on Combustion*, 2018.

[15] JF van Kampen, Jacobus BW Kok, and Th H van der Meer. Efficient retrieval of the thermo-acoustic flame transfer function from a linearized cfd simulation of a turbulent flame. *International journal for numerical methods in fluids*, 54(9):1131–1149, 2007.

[16] Mathieu Blanchard, T Schuller, D Sipp, and PJ Schmid. Response analysis of a laminar premixed m-flame to flow perturbations using a linearized compressible navier-stokes solver. *Physics of Fluids*, 27(4):043602, 2015.

[17] Energy Equation in OpenFOAM – CFD Direct. URL `https://cfd.direct/openfoam/energy-equation/{\#}x1-70004`. last visited 2017-09-27.

[18] D. C. Haworth and T. J. Poinsot. Numerical simulations of lewis number effects in turbulent premixed flames. *Journal of Fluid Mechanics*, 244:405–436, 1992. doi: 10.1017/S0022112092003124.

[19] Charles K Westbrook and Frederick L Dryer. Simplified reaction mechanisms for the oxidation of hydrocarbon fuels in flames. *Combustion science and technology*, 27(1-2):31–43, 1981.

[20] William Sutherland. Lii. the viscosity of gases and molecular force. *The London, Edinburgh, and Dublin Philosophical Magazine and Journal of Science*, 36(223):507–531, 1893. doi: 10.1080/14786449308620508.

[21] Alexander Burcat. Thermochemical data for combustion calculations. *Combustion chemistry*, pages 455–473, 1984.

[22] JANAF. NASA thermodynamic files: GRI-Mech Version 3.0 Thermodynamics. URL `http://combustion.berkeley.edu/gri_mech/version30/files30/thermo30.dat`. last visited 2017-11-07.

[23] M. Meindl, Alybayrak A., and W. Polifke. A discontinuous galerkin finite element method for thermoacoustic stability analysis based on the linearized navier-stokes equations. *submitted to J. Comp. Phys.*, 2018.